Theory of terahertz generation in a slab of electro-optic material using an ultrashort laser pulse focused to a line

M. I. Bakunov,[1,2] S. B. Bodrov,[1,2] A. V. Maslov,[3,*] and M. Hangyo[4]
[1]*Department of Radiophysics, University of Nizhny Novgorod, Nizhny Novgorod 603950, Russia*
[2]*Institute of Applied Physics, Russian Academy of Sciences, Nizhny Novgorod 603950, Russia*
[3]*NASA Ames Research Center, Mail Stop 229-1, Moffett Field, California 94035, USA*
[4]*Laser Terahertz Division, Institute of Laser Engineering, Osaka University, Osaka 565-0871, Japan*
(Received 9 April 2007; revised manuscript received 11 June 2007; published 31 August 2007)

A theory that describes the optical-to-terahertz conversion of femtosecond laser pulses via optical rectification in a slab of an electro-optic material is developed. Two typical experimental situations—phase-matched regime (ZnTe excited with 780 nm optical pump) and non-phase-matched regime ($LiNbO_3$ excited with 800 nm optical pump and GaAs excited with 1.56 μm optical pump)—are considered. The theory accounts for the transverse size of the laser beam and allows us to explore the dependence of the conversion efficiency on laser focusing. We trace the temporal dynamics of the optical-to-terahertz conversion inside the slab and study the angular distribution of the terahertz emission from the slab. The optimal parameters (such as laser transverse size and crystal thickness) maximizing the terahertz yield for ZnTe and GaAs are calculated.

DOI: 10.1103/PhysRevB.76.085346 PACS number(s): 42.65.Ky, 71.36.+c, 42.72.Ai

I. INTRODUCTION

Optical rectification of ultrashort laser pulses propagating through nonlinear crystals is a proven way to generate broadband terahertz radiation. In this technique, that was first demonstrated with picosecond pulses[1,2] and later extended to femtosecond pulses,[3,4] the pump optical pulse produces a nonlinear polarization which follows the envelope of the intensity of the pulse. This nonlinear polarization moves with the group velocity of the pulse and emits terahertz radiation. In general, one can classify the terahertz generation into two regimes, according to the dispersion properties of the material. When the group velocity of the optical pulse exceeds the highest phase velocity for terahertz waves in the material, we have superluminal (or non-phase-matched) regime. When the opposite relation holds, we have subluminal (or phase-matched) regime.[5,6]

In the superluminal regime, the optical pulse can produce terahertz radiation via Cherenkov radiation mechanism: the moving nonlinear polarization emits terahertz radiation very much like a relativistic dipole emits Cherenkov radiation.[7] To produce a Cherenkov cone of terahertz waves, the optical pulse should be focused to a size of the order of or smaller than the terahertz wavelength. Otherwise, only a quasiplane terahertz wave propagating collinearly with the laser pulse can be excited. The latter process is inefficient due to lack of phase matching between the wave and the moving source—only a thin layer of the crystal within the coherence length contributes to the generation.[8] The superluminal regime is typical, for example, for the excitation of $LiNbO_3$ with Ti:sapphire laser pulses ($\sim$800 nm wavelength)[9] and GaAs with fiber laser pulses ($\sim$1.5–2 μm wavelength).[10,11] A way to achieve the quasi-phase-matching conditions for large aperture laser beams is the use of structures with periodically inverted sign of second-order susceptibility, such as periodically poled lithium niobate (PPLN) crystal.[12] Relatively high conversion efficiencies (10^{-5}) were reached for femtosecond pulses at 800 nm in a cryogenically cooled (18 K) PPLN crystal.[13] Recently, terahertz radiation with tunable central frequency (1.78–2.49 THz) of the spectrum was generated in another quasi-phase-matched material, orientation-patterned gallium arsenide[14] (see also Ref. 15). Another way to achieve phase matching in a superluminal material is to use pump pulses with tilted fronts.[16] The operation principle has been demonstrated by generating subpicosecond pulses at approximately 2 THz in $LiNbO_3$ with a record conversion efficiency of 4.3×10^{-5} at 77 K.[17] Further improvement of the conversion efficiency up to 5×10^{-4} at room temperature was reported in Ref. 18. A disadvantage of using Cherenkov radiation in superluminal materials is the difficulty of extracting the terahertz pulses from the crystal due to total internal reflection: typically, large static dielectric constant of the crystal leads to a small critical angle and the generated pulse suffers total internal reflection at the crystal boundary.[4] To overcome this limitation, a special shaping of crystals or prism output coupling is used.[9,17–19]

In the subluminal regime, there is always a frequency at which phase matching is achieved, owing to the presence of dispersion. Indeed, in a subluminal material the phase velocity of terahertz waves in the low-frequency limit exceeds the optical group velocity and decreases with frequency, tending to zero when the frequency approaches the phonon resonance. Thus, the phase velocity coincides with the optical group velocity at some specific frequency below the phonon resonance.[5,6] This provides a simple and effective way to generate terahertz radiation: irradiation of a slab of subluminal material by a large (as compared to the terahertz wavelength) aperture beam of femtosecond laser pulses results in the phase-matched excitation of a quasiplane terahertz wave propagating collinearly to the laser beam. Nowadays, optical rectification of Ti:sapphire laser pulses in ZnTe, where phase matching with a 2 THz wave occurs, is probably the most widely used technique for the generation of broadband terahertz pulses.[20,21]

Although the classification of terahertz generation as subluminal (phase-matched) and superluminal (Cherenkov or

non-phase-matched) regimes is convenient for wide optical beams, there is no principal difference between the two regimes for focused beams. In fact, in the superluminal regime, phase matching is achieved between a strongly focused moving optical pulse and a plane terahertz wave propagating under some angle with respect to the laser path. Due to dispersion, a continuum of plane waves with different frequencies and different propagating angles is excited by the pulse. If the laser pulse with a transverse size comparable to or smaller than the terahertz wavelength propagates in a subluminal material, two mechanisms mix—both the collinearly and obliquely propagating terahertz waves are generated behind the pulse (see also Ref. 6).

Despite the presence of a large number of experimental results on optical rectification in electro-optic crystals, the theory of this phenomenon has still not been developed sufficiently even in the limit of low pump intensities, and even less for intensities at which higher-order nonlinear effects, such as two-photon absorption and self-focusing, become essential. Theoretical treatments of the phase-matched and quasi-phase-matched regimes are typically restricted to the simple one-dimensional (1D) or plane-wave approximation (see, for example, Refs. 12 and 21–24). This model does not allow one to study correctly the role of laser focusing. In particular, a 1D analysis predicts that the optical-to-terahertz conversion efficiency is proportional to the optical intensity and, therefore, inversely proportional to the illuminated emitter area at a fixed laser pulse energy.[21] This prediction fails, however, when the laser transverse size becomes comparable to the terahertz wavelength. According to calculations of Ref. 11 for the regime of quasi-phase-matching in GaAs, the growth of conversion efficiency slows down with further decrease of the optical spot area and then saturates (see also Ref. 25 where the influence of focusing on the difference-frequency generation of two monochromatic laser beams was analyzed). Moreover, if the optical width becomes smaller than the terahertz wavelength, experiments show a decrease in the generated terahertz power.[18,26–28] The use of Bethe's theory of the electromagnetic wave penetration through a small aperture[22,26] to explain the decrease seems only weakly relevant (see also Ref. 28). In addition, the mentioned 1D calculations often neglect the dispersion of terahertz waves.

Another essential drawback of many existing theoretical approaches is how the crystal boundaries are included into the problem. At the entrance surface of the crystal, an incorrect boundary condition of vanishing terahertz field is often assumed (see, for example, Refs. 22–24 and 29). At the end of the crystal, no matching of the terahertz waves generated inside the crystal to free-space terahertz radiation was performed either. Reference 30 presented a general formalism that included all three essential effects, i.e., finite width of the laser beam, medium dispersion, and transmission through the crystal boundary, but did not discuss sufficiently the role of these effects for terahertz generation.

As for the theory of Cherenkov emission of terahertz waves by optical pulses, it was developed only for coherent phonon polaritons generated in infinite crystals.[6,31] The transformation of phonon polaritons to free-space terahertz radiation at the crystal boundary was not considered. In addition, Ref. 31 neglected important effects such as medium dispersion and absorption. A recent paper[6] included dispersion but not the energy characteristics (such as total radiated energy per unit length of the laser path and spectral-angular distribution of the radiated energy) of Cherenkov radiation.

We set two goals in this paper. The first is to develop a comprehensive theory of optical-to-terahertz conversion in a slab of nonlinear material that includes all essential factors, such as finite width of the laser beam, medium dispersion, and the presence of the crystal boundaries. The second is to apply this theory to typical experimental materials. The theory is based on an exact solution of Maxwell's equations for terahertz fields excited by a nonlinear source. The two-dimensional (2D) case when the pump laser pulse is infinite in one direction and has a finite width in the other direction is considered. The 2D case does not require very bulky numerical calculations as the three-dimensional case of focusing to a spot. At the same time, it allows us to study the influence of laser focusing on the conversion efficiency. Besides being a natural step in generalizing the simplest (one-dimensional) plane-wave approximation, the 2D case has significant practical importance. Recently, focusing pump laser pulses into a line by a cylindrical lens was proposed as a means to increase the energy of the terahertz pulses.[32] Such focusing can provide several advantages for the construction of powerful terahertz sources.[32] First, the terahertz radiation emitted by a line-source setup forms two beams having nearly flat phase fronts. This terahertz pattern is more convenient for practical applications as compared to the Cherenkov cone produced by the laser focused to a spot. Second, when focusing to a spot, its size, on the one hand, should be smaller than the terahertz wavelength to produce Cherenkov radiation and, on the other hand, the laser intensity cannot exceed the damage threshold of the crystal. These two conditions limit the maximum energy of the generated terahertz pulse. In the case of focusing into a line, the terahertz pulse energy can be easily increased by using laser pulses with higher energy and increasing the length of the line in order to keep the laser intensity below the threshold. In experiments, the line-source geometry provided a conversion efficiency of 1.7×10^{-5} for 2 μJ Ti:sapphire pump laser pulses in $LiNbO_3$ at room temperature.[32] In Ref. 18, the energies of the terahertz pulses generated by line focusing and front tilting were similar for pump energies up to 32 μJ. Although line focusing is quite often used today, a similar idea (to use two perfectly conducting sheets as a means to confine the Cherenkov radiation in a thin slab) was proposed a long time ago in Ref. 34. Later, the line-source geometry was used for generating phonon polaritons in $LiTaO_3$.[33] Recently, we proposed the use of striplike optical spots moving along semiconductor surfaces to generate surface plasmon polaritons at the terahertz frequencies.[35–37]

After deriving general formulas to describe the terahertz radiation, we consider two typical experimental situations: (a) non-phase-matched case ($LiNbO_3$ at 800 nm and GaAs at 1.56 μm) and (b) phase-matched case (ZnTe excited with 780 nm optical pump). We study the temporal dynamics of the optical-to-terahertz conversion inside the slab and the angular distribution of the terahertz emission from the slab. The theory allows us to explore the dependence of the conversion efficiency on laser focusing. The optimal parameters

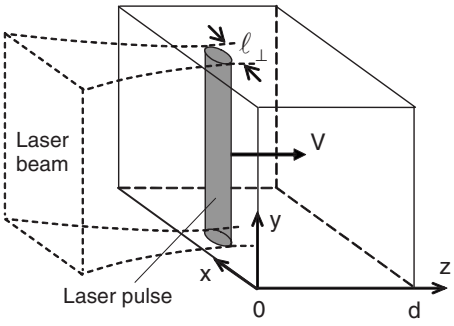

FIG. 1. Geometry of the problem: An optical pulse focused to a line is incident on a slab of nonlinear material.

(such as laser transverse size and crystal thickness) maximizing the terahertz yield for GaAs and ZnTe are then calculated.

II. MODEL AND BASIC EQUATIONS

Let us consider a slab of nonlinear material of thickness d and choose the system of coordinates as shown in Fig. 1. We assume that the interface $z=0$ of the slab is illuminated normally by a femtosecond laser pulse focused in the x direction by a cylindrical lens. The beam width in this direction $\ell_\perp$ can be varied in a wide range as in a typical experimental situation of Z-scan measurements. In the y direction, the beam width is assumed to be much greater than the terahertz wavelength. This allows us to approximate it by a two-dimensional pulse with fields independent of y. The pulse propagates through the slab with a group velocity $V=c/n_g$, where n_g is the optical group refractive index and we neglect the distortion of the pulse due to dispersion. Diffractive broadening of the pulse is also neglected since experimentally used slabs are thinner than the Rayleigh length for the laser beam. We neglect the pulse depletion due to linear absorption (typically weak in crystals such as ZnTe, GaAs, and $LiNbO_3$ below the band gap) and due to nonlinear processes, such as two-photon absorption and second-harmonic generation. The latter is a reasonable approximation at not very high pump intensities we are interested in here. We do not account for the pulse reflection from the interface $z=d$ because the reflected pulse moving in the $-z$ direction will produce mainly the terahertz radiation propagating in this backward direction. Using all the mentioned approximations, we write the nonlinear polarization induced in the slab via optical rectification as

$$\mathbf{P}^{\mathrm{NL}} = \mathbf{p}F(\xi)G(x)\Pi(z), \tag{1}$$

where the function $\Pi(z)=1$ inside the slab $(0<z<d)$ and $\Pi(z)=0$ elsewhere. The function $G(x)$ describes the transverse profile of the optical beam; $F(\xi)$ is the time-dependent envelope of the optical intensity, and $\xi=t-z/V$. To specify our final formulas, we will use the Gaussian functions

$$G(x) = e^{-x^2/\ell_\perp^2}, \quad F(\xi) = e^{-\xi^2/\tau^2}, \tag{2}$$

where τ is the pulse duration [the standard full width at half maximum (FWHM) is $\tau_{\mathrm{FWHM}}=2\sqrt{\ln 2}\tau$]. We will also use

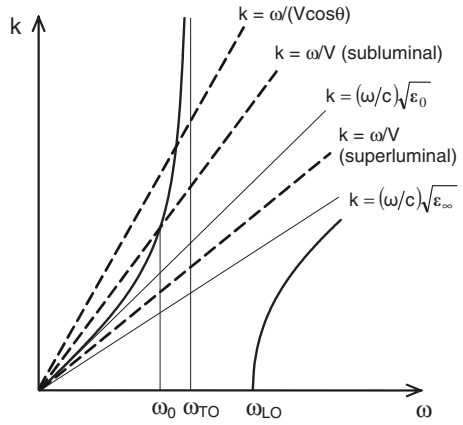

FIG. 2. Kinematic diagram (wave number k vs frequency ω) which illustrates the difference between superluminal and subluminal regimes. The intersection of the dispersion curve for terahertz waves [plotted based on Eq. (4) using bold solid lines] and the line $k=\omega/V$ gives the frequency ω_0 at which phase matching between the moving source and the wave propagating along the z axis is achieved. The intersection with the line $k=\omega/(V\cos\theta)$ gives the frequency of the partial (phase-matched) plane wave propagating at an angle θ to the z axis.

$\ell_{\perp\mathrm{FWHM}}=2\sqrt{\ln 2}\ell_\perp$. The orientation of the amplitude vector $\mathbf{p}$ is determined by the polarization of the optical beam and orientation of the crystallographic axes of the sample. We will include all three components: p_x, p_y, and p_z.

To find the terahertz radiation generated by the moving nonlinear polarization [Eq. (1)], we use Maxwell's equations (all formulas in the paper are given in cgs):

$$\nabla \times \mathbf{E} = -\frac{1}{c}\frac{\partial \mathbf{B}}{\partial t}, \tag{3a}$$

$$\nabla \times \mathbf{B} = \frac{1}{c}\frac{\partial \mathbf{D}}{\partial t} + \frac{4\pi}{c}\frac{\partial \mathbf{P}_{\mathrm{NL}}}{\partial t}. \tag{3b}$$

These equations should be supplemented by a constitutive relation in the terahertz range. This relation between vectors $\mathbf{D}$ and $\mathbf{E}$ can be conveniently written in the frequency domain (see Sec. IV).

III. KINEMATICS OF TERAHERTZ WAVE EXCITATION

Let us discuss briefly the two possible regimes—superluminal and subluminal—of terahertz wave excitation (see Fig. 2) which are determined by the relation between the phase velocities of terahertz waves and group velocity of the optical pulse. The phase velocities of terahertz waves can be found using the dielectric constant which has the following form in the one-phonon-resonance approximation:

$$\varepsilon = \varepsilon_\infty + \frac{(\varepsilon_0 - \varepsilon_\infty)\omega_{\mathrm{TO}}^2}{\omega_{\mathrm{TO}}^2 - \omega^2 + i\gamma\omega}, \tag{4}$$

where ε_0 and ε_∞ are the low- and high-frequency dielectric constants, respectively, ω_{TO} is the transverse optical phonon frequency, and γ is the damping rate. The resultant disper-

sion curve has two branches, as shown in Fig. 2. We will focus only on the lower-frequency branch (below ω_{TO}) which is typically studied in experiments on terahertz generation. The excitation of the higher-frequency branch (above the longitudinal optical phonon frequency ω_{LO}) requires very short and fast optical pulses ($V > c/\sqrt{\varepsilon_\infty}$) and will be discussed briefly in Sec. VI.

In the superluminal regime, the group velocity of the optical pulse (and thus, of the pulse of nonlinear polarization [Eq. (1)]) is larger than the phase velocity of the fastest (low-frequency) terahertz waves propagating along z, i.e., $V > c/\sqrt{\varepsilon_0}$. However, phase matching can be achieved for a continuum of terahertz waves propagating at finite angles θ with respect to z. The generated terahertz radiation has a broad spectrum ($0 < \omega < \omega_{TO}$) and forms a Cherenkov cone. Such excitation, however, occurs only if the optical beam is strongly focused (compared to the terahertz wavelength); a wide laser pulse can only generate near fields.

If the velocity of the optical pulse decreases and approaches $c/\sqrt{\varepsilon_0}$, the opening of the Cherenkov cone increases until it reaches $\pi/2$. If the pulse becomes even slower ($V < c/\sqrt{\varepsilon_0}$, subluminal regime), the excited terahertz spectrum becomes limited from below by the frequency ω_0 (Fig. 2) of the terahertz component that propagates along the z axis ($\theta = 0$). A strongly focused optical pulse can generate a full spectrum ($\omega_0 < \omega < \omega_{TO}$) of terahertz waves propagating at $0 < \theta < \pi/2$. This is similar to the superluminal regime. In contrast, a weakly focused pulse excites predominantly the forward-propagating terahertz wave. This strong dependence of the excitation picture poses a question of optimal pulse focusing to achieve the highest possible optical-to-terahertz conversion.

The discussion of the excitation regimes presented above is relevant to the stationary regime, i.e., when the optical pulse propagates in a homogeneous material. In practical situations, the optical laser pulse excites transiently all waves allowed by the dispersion curve upon its entrance into the crystal. This transient radiation can significantly affect the total terahertz field. We will address this issue in Sec. VI.

IV. GENERAL SOLUTION

To solve Eqs. (3), we apply Fourier transforms with respect to t and x to these equations and use the constitutive relation between the Fourier transforms of the electric field and displacement vector (ω and g are the Fourier variables which correspond to t and x, respectively; $\tilde{}$ will denote quantities in the Fourier domain): $\tilde{\mathbf{D}}(z,g,\omega) = \varepsilon(z,\omega)\tilde{\mathbf{E}}(z,g,\omega)$, where the complex dielectric function $\varepsilon(z,\omega)$ is $\varepsilon_c(\omega)$ inside the crystal ($0 < z < d$) and unity in vacuum. We do not need to specify $\varepsilon_c(\omega)$ at this point. This will be done in Sec. VI for specific materials.

Equations (3) written in the Fourier domain and projected into the coordinate system can be separated into two independent sets—for s-polarized waves (field components $\tilde{E}_y$, $\tilde{B}_x$, and $\tilde{B}_z$) and p-polarized waves (field components $\tilde{B}_y$, $\tilde{E}_x$, and $\tilde{E}_z$).

For s-polarized waves, eliminating $\tilde{B}_x$ and $\tilde{B}_z$ using

$$\tilde{B}_x = \frac{c}{i\omega}\frac{\partial \tilde{E}_y}{\partial z}, \quad \tilde{B}_z = \frac{cg}{\omega}\tilde{E}_y, \tag{5}$$

we obtain an equation for $\tilde{E}_y$:

$$\frac{\partial^2 \tilde{E}_y}{\partial z^2} + \kappa^2 \tilde{E}_y = -\frac{4\pi\omega^2 p_y}{c^2}\tilde{F}(\omega)\tilde{G}(g)\Pi(z)e^{-i\omega z/V}. \tag{6}$$

For p-polarized waves, eliminating $\tilde{E}_x$ and $\tilde{E}_z$ using

$$\tilde{E}_x = \frac{ic}{\omega\varepsilon}\frac{\partial \tilde{B}_y}{\partial z} - \frac{4\pi p_x}{\varepsilon}\tilde{F}\tilde{G}\Pi(z)e^{-i\omega z/V}, \tag{7a}$$

$$\tilde{E}_z = -\frac{cg}{\omega\varepsilon}\tilde{B}_y - \frac{4\pi p_z}{\varepsilon}\tilde{F}\tilde{G}\Pi(z)e^{-i\omega z/V}, \tag{7b}$$

we obtain an equation for $\tilde{B}_y$:

$$\varepsilon\frac{\partial}{\partial z}\left(\frac{1}{\varepsilon}\frac{\partial \tilde{B}_y}{\partial z}\right) + \kappa^2 \tilde{B}_y = -\frac{4\pi i\omega}{c}\tilde{F}(\omega)\tilde{G}(g)\left\{p_x\varepsilon\frac{\partial}{\partial z}\left[\frac{1}{\varepsilon}\Pi(z)e^{-i\omega z/V}\right] + p_z ig\Pi(z)e^{-i\omega z/V}\right\}. \tag{8}$$

In Eqs. (6) and (8), we introduced the longitudinal wave vector $\kappa(z,g,\omega)$ given by

$$\kappa^2 = (\omega/c)^2\varepsilon(z,\omega) - g^2 \tag{9}$$

and the Fourier transforms $\tilde{F}(\omega) = (\tau/2\sqrt{\pi})e^{-\omega^2\tau^2/4}$ and $\tilde{G}(g) = (\ell_\perp/2\sqrt{\pi})e^{-g^2\ell_\perp^2/4}$ of the envelope $F(\xi)$ and beam profile $G(x)$, respectively.

We proceed by solving Eqs. (6) and (8) in the homogeneous regions ($z < 0$, $0 < z < d$, and $z > d$) and matching the solutions by the boundary conditions of continuity $\tilde{E}_y$ and $\tilde{B}_x$ for s-polarized waves and $\tilde{B}_y$ and $\tilde{E}_x$ for p-polarized waves.

For s-polarized waves, matching gives the following expressions for the electric field transform:

$$\tilde{E}_y = \begin{cases} C_1 e^{i\kappa_v z}, & z < 0 \\ C_2 e^{-i\kappa_c z} + C_3 e^{i\kappa_c z} - A e^{-i\omega z/V}, & 0 < z < d \\ C_4 e^{-i\kappa_v (z-d)}, & z > d \end{cases} \tag{10}$$

with

$$A = 4\pi p_y \tilde{F}\tilde{G}/(c^2\kappa_c^2/\omega^2 - n_g^2), \tag{11a}$$

$$C_1 = C_2 + C_3 - A, \tag{11b}$$

$$C_4 = C_2 e^{-i\kappa_c d} + C_3 e^{i\kappa_c d} - A e^{-i\omega d/V}, \tag{11c}$$

$$C_{2,3} = A[(\kappa_c \pm \kappa_v)(\kappa_v + \omega/V)e^{\pm i\kappa_c d} + (\kappa_c \mp \kappa_v) \times (\kappa_v - \omega/V)e^{-i\omega d/V}]/\Delta_s, \tag{11d}$$

$$\Delta_s = (\kappa_c + \kappa_v)^2 e^{i\kappa_c d} - (\kappa_c - \kappa_v)^2 e^{-i\kappa_c d}. \tag{11e}$$

The coefficient κ_v is κ taken with $\varepsilon=1$ and κ_c is κ taken with $\varepsilon=\varepsilon_c$ [see Eq. (9)].

For p-polarized waves, matching gives the following expressions for the magnetic field transform:

$$\tilde{B}_y = \begin{cases} D_1 e^{i\kappa_v z}, & z<0 \\ D_2 e^{-i\kappa_c z} + D_3 e^{i\kappa_c z} - R e^{-i\omega z/V}, & 0<z<d \\ D_4 e^{-i\kappa_v (z-d)}, & z>d \end{cases} \tag{12}$$

with

$$R = 4\pi(p_x n_g - p_z c g/\omega)\tilde{F}\tilde{G}/(c^2\kappa_c^2/\omega^2 - n_g^2), \tag{13a}$$

$$D_1 = D_2 + D_3 - R, \tag{13b}$$

$$D_4 = D_2 e^{-i\kappa_c d} + D_3 e^{i\kappa_c d} - R e^{-i\omega d/V}, \tag{13c}$$

$$D_{2,3} = \{(\kappa_c \pm \varepsilon_c\kappa_v)[R(\varepsilon_c\kappa_v + \omega/V) + Q]e^{\pm i\kappa_c d} + (\kappa_c \mp \varepsilon_c\kappa_v) \times [R(\varepsilon_c\kappa_v - \omega/V) - Q]e^{-i\omega d/V}\}/\Delta_p, \tag{13d}$$

$$Q = 4\pi\omega p_x \tilde{F}\tilde{G}/c, \tag{13e}$$

$$\Delta_p = (\kappa_c + \varepsilon_c\kappa_v)^2 e^{i\kappa_c d} - (\kappa_c - \varepsilon_c\kappa_v)^2 e^{-i\kappa_c d}. \tag{13f}$$

With the solution in the Fourier domain at hand, Eqs. (10)–(13), we can transform it to the t, x domain by taking the inverse transforms in the form

$$E_y(z,x,t) = \int_{-\infty}^{\infty} d\omega \int_{-\infty}^{\infty} dg e^{i\omega t - igx} \tilde{E}_y(z,g,\omega) \tag{14}$$

and the same formulas used for the other fields. Our numerical calculations of radiation patterns and oscillograms for specific materials in Sec. VI will be based on this formula.

To find the energy (per unit length of the line source) emitted from the slab in the forward direction, we integrate the z component of the Poynting vector $S_z=-(c/4\pi)E_y B_x$ and $S_z=(c/4\pi)E_x B_y$ for s and p polarizations, respectively, taken at $z>d$ over infinite intervals $-\infty<x<+\infty$ and $-\infty<t<+\infty$. This yields the total energies $W_{s,p}$ radiated in the $+z$ direction, for s and p polarizations, respectively, in the form

$$W_{s,p} = \int_{-\pi/2}^{\pi/2} d\theta \int_0^{\infty} d\omega w_{s,p}(\theta,\omega), \tag{15}$$

where the spectral-angular density of energy is

$$w_{s,p}(\theta,\omega) = 2\pi\omega\cos^2\theta \begin{cases} |C_4(g,\omega)|^2, & s\text{-waves} \\ |D_4(g,\omega)|^2, & p\text{-waves}, \end{cases} \tag{16}$$

and angle θ is measured in the x, z plane with respect to the $+z$ direction. When substituting Eqs. (11c) and (13c) for $C_4(g,\omega)$ and $D_4(g,\omega)$ into Eq. (16), the transverse wave number g should be expressed in terms of ω and θ using $g=(\omega/c)\sin\theta$. The waves, emitted at a fixed θ, have a continuous spectrum, according to Eqs. (15) and (16), so that the angular density of the radiated energy can be found by integrating $w_{s,p}(\theta,\omega)$ over ω: $w_{s,p}(\theta)=\int_0^{\infty} d\omega w_{s,p}(\theta,\omega)$.

Equations (15) and (16) give the total terahertz energy emitted from the slab in the forward direction including the terahertz pulses that experience double and multiple reflections from the slab's boundaries and arrive at the detector with a periodic delay. In practice, however, only the first (direct) terahertz pulse is typically used. To filter out the rereflected pulses in our numerical calculations below, we integrate the Poynting vector over a time window that is greater than the duration of the first terahertz pulse but smaller than the round-trip time in the slab. Those time scales are well separated for slab thicknesses $d>100$ μm typically used in experiments. The contribution of the rereflected pulses into the radiated energy is small ($\leq 10\%$ in the examples below) but it would lead to undesirable interference fringes in the generated spectrum.

V. TERAHERTZ GENERATION IN A SEMI-INFINITE MATERIAL

To get an analytical insight into the process of terahertz generation in the crystal, let us set aside for a while the effects that arise from the presence of the exit surface of the crystal at $z=d$ and consider first the limiting case of a semi-infinite crystal ($d\to\infty$). The main differences between the solutions for s- and p-polarized waves arise from their different transmissions to vacuum. Since effects related to the end transmission are not the subject of this section, we will focus here on the simpler case of s polarization. In the limit $d\to\infty$, Eqs. (11b) and (11d) for $C_{1,2,3}$ are simplified to $C_1=C_2-A$, $C_2=A(\kappa_v+\omega/V)/(\kappa_v+\kappa_c)$, and $C_3=0$, and the electric field transform in the crystal becomes

$$\tilde{E}_y(z,g,\omega) = A\left(\frac{\kappa_v + \omega/V}{\kappa_v + \kappa_c} e^{-i\kappa_c z} - e^{-i\omega z/V}\right), \tag{17}$$

where A is still given by Eq. (11a). Equation (17) consists of free-wave (the first term) and forced-wave (second term) responses.

A. Planar optical pulse

In the planar source limit ($\ell_\perp\to\infty$), the function $\tilde{G}(g)$ in the coefficient A transforms to the delta function $\delta(g)$: $\tilde{G}(g)\to\delta(g)$. Substitution of Eq. (17) into Eq. (14) gives

$$E_y(z,t) = 4\pi p_y \int_{-\infty}^{\infty} d\omega \frac{\tilde{F}(\omega)}{\varepsilon_c(\omega) - n_g^2} \times \left[\frac{1+n_g}{1+\sqrt{\varepsilon_c(\omega)}} e^{i\omega(t-\sqrt{\varepsilon_c(\omega)}z/c)} - e^{i\omega(t-z/V)}\right]. \tag{18}$$

In Eq. (18), the free-wave response (first term in the brackets) propagates with distortion due to dispersion and absorption. The forced-wave response (second term in the brackets) propagates without changing its shape.

In the superluminal regime, when $n_g^2<\varepsilon_c(\omega)$, the integrand in Eq. (18) has no peculiarity. Therefore, as a first approximation, we can neglect the dispersion and absorption

in the terahertz range and consider $\sqrt{\varepsilon_c(\omega)}$ as a real constant n_t (more accurately, an additional condition on the pulse duration $\omega_{\mathrm{TO}}\tau_{\mathrm{FWHM}} \gg 1$ is required to avoid the distortion of the spectrum in the vicinity of ω_{TO} and the excitation of the upper polariton branch). This allows us to evaluate the integral (18) analytically:

$$E_y(z,t) = \frac{4\pi p_y}{n_t^2 - n_g^2}\left[\frac{1+n_g}{1+n_t}F\left(t - \frac{zn_t}{c}\right) - F\left(t - \frac{z}{V}\right)\right]. \quad (19)$$

Equation (19) predicts the generation of two terahertz pulses of the same (Gaussian) shape, which mimics the envelope of optical intensity, but with different amplitudes and opposite signs. The pulses propagate with different velocities: the forced-wave response propagates with the velocity of the pump laser pulse (i.e., the optical group velocity) and the free-wave response propagates with the group velocity in the terahertz range. From the physical point of view, the forced-wave response is near field and the free-wave response is free-space radiation. Near the entrance surface of the crystal ($z=0$), the pulses coincide in time and partially compensate each other; in the course of propagation they become separated and, therefore, the total terahertz field increases. Thus, it is convenient to introduce a walk-off length as the position inside the crystal at which the total terahertz field shows two separate pulses as a function of time. This walk-off length is

$$L_w = \frac{c}{n_t - n_g}\tau_{\mathrm{FWHM}}. \quad (20)$$

The introduced walk-off length should be distinguished from the so-called coherence length that characterizes the interaction of a moving source with a specific terahertz harmonic.[20] Although the walk-off length was introduced earlier in Ref. 11, our Eq. (20) and preceding discussion give a more accurate definition for the walk-off length and clarify its physical meaning. Interestingly, the separation of the two terahertz pulses in space is characterized by another walk-off length $L_w^{\mathrm{space}} = (c\tau_{\mathrm{FWHM}}/2)(1+n_t/n_g)/(n_t - n_g)$ that can differ significantly from L_w given by Eq. (20) if $n_g \ll n_t$. The walk-off length L_w^{space} gives the position of the optical pulse when the two pulses become separated spatially at some specific moment of time. We will use L_w^{space} to interpret the snapshots in Sec. VI.

While the amplitude of the forced-wave pulse does not change for $z > L_w$, dispersion and absorption, if taken into account, should lead to gradual distortion and fading of the free-wave pulse. The generation of two terahertz pulses was predicted earlier in Refs. 22 and 24; however, Eq. (19) defines more correctly the amplitudes of the pulses. In particular, unlike Refs. 22 and 24, Eq. (19) predicts a nonzero total terahertz field at $z=0$.

For a more careful analysis of Eq. (19), it is useful to distinguish two limiting regimes for superluminal materials: strongly superluminal regime, when $n_g^2 \ll \varepsilon_0$ like in $LiNbO_3$ (see parameters in Sec. VI), and weakly superluminal regime, when n_g^2 is only slightly less than ε_0 ($n_g^2 \simeq \varepsilon_0$) like in GaAs (Sec. VI). In the strongly superluminal regime, the forced-wave pulse, according to Eq. (19), significantly exceeds the free-wave pulse in amplitude and, therefore, a finite total terahertz field, approximately equal to the forced-wave response, appears just after the optical pulse enters the crystal. Besides that, due to significant difference in the velocities of the forced- and free-wave responses, they split up at a small distance, smaller than the laser pulse length ($L_w \approx c\tau_{\mathrm{FWHM}}/n_t \ll c\tau_{\mathrm{FWHM}}/n_g$), from the entrance surface $z=0$ and propagate further separately.

In the weakly superluminal regime, the pulses have almost equal amplitudes and practically cancel each other near $z=0$; the total terahertz field gradually grows with z from zero and until the pulses become separated, i.e., within the walk-off length L_w. The latter is comparatively large in this regime [$L_w = c\tau_{\mathrm{FWHM}}/(n_t - n_g) \gg c\tau_{\mathrm{FWHM}}/n_g$] due to small difference in the velocities of the pulses. For $0 < z < L_w$, Eq. (19) can be reduced to

$$E_y \approx -\frac{4\pi p_y z}{c(n_t + n_g)}\frac{dF}{d\xi}. \quad (21)$$

This means that the total terahertz field is proportional to the derivative of the optical pulse intensity envelope taken with negative sign and the passed distance z. The maximum value of the terahertz field is

$$|E_y|_{\max} \approx \frac{4\sqrt{2}\pi p_y z}{c(n_t + n_g)\tau}e^{-1/2} \quad (22)$$

at $\xi = \pm\tau/\sqrt{2}$. For a fixed energy of the optical pulse, $p_y \propto \tau^{-1}$ in Eq. (22) and $|E_y|_{\max} \propto \tau^{-2}$. Respectively, the energy of the terahertz field scales as $\propto \tau^{-3}$. For $z > L_w$, when the forced- and free-wave pulses become entirely separated, their amplitudes should be significantly greater than the amplitudes of the pulses in the strongly superluminal regime due to smallness of the denominator in Eq. (19) at $n_g \simeq n_t$. Moreover, since the denominator $\varepsilon_c(\omega) - n_g^2$ in Eq. (18) varies significantly with frequency in the weakly superluminal regime, the low frequencies will be pronounced in the terahertz spectrum.

In the subluminal regime, there is a peculiarity in the integrand in Eq. (18) and, therefore, dispersion cannot be neglected. Calculations for this regime will be done in Sec. VI for ZnTe. Here, we focus on the derivation of an analytical formula for the forced-wave response that is the limiting form of the terahertz pulse at large distances z where the free-wave response is completely extinguished by absorption. Extending integration in Eq. (18) to the complex ω plane, one can represent the forced-wave response as a sum of two terms: near field of the moving source and radiation behind the source. The latter is given by residue contributions from the poles defined by the equation $\varepsilon_c(\omega) - n_g^2 = 0$. Using the one-phonon-resonance formula (4) for $\varepsilon_c(\omega)$, we find the positions of the poles, $\omega = \pm\omega_0 + i\gamma/2$, where

$$\omega_0 = \omega_{\mathrm{TO}}\sqrt{(n_g^2 - \varepsilon_0)/(n_g^2 - \varepsilon_\infty) - \gamma^2/(4\omega_{\mathrm{TO}}^2)}, \quad (23)$$

and then calculate the residue contributions:

$$E_y(z,t) = \frac{4\pi^{3/2} p_y (\varepsilon_0 - \varepsilon_\infty)\omega_{\mathrm{TO}}^2 \tau}{\omega_0 (n_g^2 - \varepsilon_\infty)^2} e^{-(\omega_0^2 - \gamma^2/4)\tau^2/4} e^{-\gamma\xi/2} \times \sin(\omega_0 \xi - \gamma\omega_0 \tau^2/4). \quad (24)$$

Equation (24) describes a quasimonochromatic wave packet propagating behind the laser pulse with the same velocity V and decaying with decrement $\gamma/(2V)$ with distance from the pulse. According to Eq. (24), the optimal duration of the laser pulse, that maximizes the terahertz field magnitude, is given by $\tau\sqrt{\omega_0^2 - \gamma^2/4} = \sqrt{2}$, or $\omega_0\tau \approx \sqrt{2}$ for small damping. However, the optimal pulse duration is relevant only to the case when p_y is independent of τ, i.e., for a fixed optical intensity. For a fixed energy of the optical pulse, $p_y\tau = \mathrm{const}$ in Eq. (24) and thus τ affects the terahertz field magnitude only via the Gaussian factor. Thus, shortening of the optical pulse increases the generated terahertz field. This increase, however, saturates at $\tau < \omega_0^{-1}$ (for example, at $\tau < 60$ fs, or $\tau_{\mathrm{FWHM}} < 100$ fs, for $\omega_0 = 2.5$ THz). Since the length of the terahertz wave packet is independent of τ, the terahertz energy similarly exhibits the dependence on τ only via the Gaussian factor and saturates at $\tau < \omega_0^{-1}$ (see also Ref. 11).

It is interesting to compare Eq. (18) with the corresponding expression that follows from the slowly varying envelope approximation (SVEA) (see, for example, Ref. 11):

$$E_y^{\mathrm{SVEA}}(z,t) = 2\pi p_y \int_{-\infty}^{\infty} d\omega \frac{\tilde{F}(\omega)}{\sqrt{\varepsilon_c(\omega)}(\sqrt{\varepsilon_c(\omega)} - n_g)} \times [e^{i\omega(t - \sqrt{\varepsilon_c(\omega)}z/c)} - e^{i\omega(t - z/V)}]. \quad (25)$$

In the superluminal regime, neglecting the dispersion ($\sqrt{\varepsilon_c(\omega)} \to n_t$) in Eq. (25) gives

$$E_y^{\mathrm{SVEA}}(z,t) = \frac{2\pi p_y}{n_t(n_t - n_g)} \left[F\left(t - \frac{z n_t}{c}\right) - F\left(t - \frac{z}{V}\right) \right]. \quad (26)$$

Comparing Eq. (26) with the more accurate Eq. (19), we conclude that using SVEA leads to significant errors in the amplitudes of the free-wave and forced-wave responses if n_t and n_g differ significantly (for example, as in $LiNbO_3$, see parameters in Sec. VI). For similar values of n_t and n_g or in the subluminal regime, as we carefully checked for GaAs and ZnTe (Sec. VI), the SVEA formula (25) works very well.

B. Focused optical pulse

For an arbitrary transverse size of the laser beam, the limiting form of the generated terahertz field at large z can be found by substituting the forced-wave response (second term) from Eq. (17) to Eq. (14). In the inner integral on g of Eq. (14), we close the integration contour in the lower half-plane of the complex g plane for $x > 0$ and in the upper half-plane for $x < 0$. The contours are similar to that we used earlier in Refs. 35 and 38, but without any branch cuts. The residue contributions to the integral from the poles given by $g^2 - (\omega/c)^2[\varepsilon_c(\omega) - n_g^2] = 0$ define the Cherenkov cone; the contributions from the semi-infinite straight lines tilted at an angle of 45° with the axes (see Refs. 35 and 38) give the near field of the moving source. Thus, unlike the limit of a planar laser pulse, the forced-wave response consists of both the near field and the Cherenkov cone. Taking into account only the residue contributions and, thus, neglecting the near field, we obtain (assuming for simplicity $\gamma = 0$)

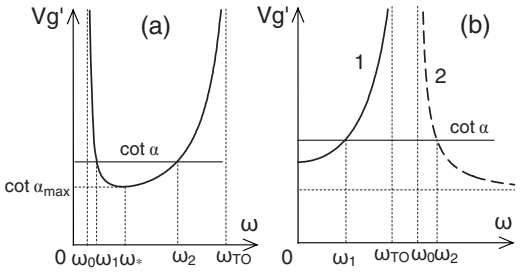

FIG. 3. Graphical solution of Eq. (29). In the subluminal regime (a), there are two roots $\omega_{1,2}$ for $\alpha < \alpha_{\max}$; these roots merge at ω_* for $\alpha = \alpha_{\max}$. In the superluminal regime (b), there is only one root ω_1 if $\varepsilon_\infty < n_g^2 < \varepsilon_0$ [curve 1 starts from $(\varepsilon_0/n_g^2 - 1)^{1/2}$ at $\omega = 0$]; the second root ω_2 appears from the upper branch (curve 2) for $n_g^2 < \varepsilon_\infty$ [curve 2 tends to $(\varepsilon_\infty/n_g^2 - 1)^{1/2}$ at $\omega \to \infty$].

$$E_y(z,x,t) = \frac{8\pi^2 p_y}{c^2} \int_{\varepsilon_c(\omega) > n_g^2} d\omega \frac{\omega^2}{g} \tilde{F}(\omega)\tilde{G}(g) \sin(\omega\xi - g|x|), \quad (27)$$

with $g = (\omega/c)[\varepsilon_c(\omega) - n_g^2]^{1/2}$. Integration in Eq. (27) goes over the intervals of positive ω where $\varepsilon_c(\omega) > n_g^2$. For $\varepsilon_c(\omega)$ given by Eq. (4) with $\gamma = 0$, the intervals are as follows: (i) $\omega_0 < \omega < \omega_{\mathrm{TO}}$ in the subluminal regime ($n_g^2 > \varepsilon_0$), (ii) $0 < \omega < \omega_{\mathrm{TO}}$ in the superluminal regime with $\varepsilon_\infty < n_g^2 < \varepsilon_0$, or (iii) $0 < \omega < \omega_{\mathrm{TO}}$ and $\omega_0 < \omega < \infty$ in the superluminal regime with $n_g^2 < \varepsilon_\infty$ [ω_0 is given by Eq. (23) at $\gamma = 0$].

Integral (27) can be asymptotically evaluated for large ξ using the stationary phase method:

$$E_y(z,x,t) \approx \frac{8\pi^2 p_y}{c^2} \sum_i \frac{\omega_i^2}{g_i} \sqrt{\frac{\pi}{|g_i'' x|}} \tilde{F}(\omega_i)\tilde{G}(g_i) \times \sin\left[\omega_i \xi - g_i|x| - \frac{\pi}{4} \mathrm{sgn}(g_i'') \right], \quad (28)$$

where g_i'' denotes the second derivative with respect to ω taken at ω_i, and the sum is taken over the frequencies ω_i for which

$$V\frac{dg}{d\omega} = \frac{V\xi}{|x|} = \cot\alpha, \quad (29)$$

where α is a half-apex angle of a cone with its apex on the moving laser pulse $\xi = 0$.[6,46]

In the subluminal regime, Eq. (29) has two roots $\omega_{1,2}$ for a fixed cone with angle $\alpha < \alpha_{\max}$ [Fig. 3(a)]; the maximum angle $\alpha_{\max}$ in Fig. 3(a) corresponds to the horizontal tangent to the curve $Vg'(\omega)$ ($g' = dg/d\omega$) at its minimum where $\omega = \omega_*$. A superposition of two harmonic oscillations with frequencies ω_1 and ω_2 should give the beats in the field distribution along the cone. The beat frequency decreases with increasing α as the two roots $\omega_{1,2}$ move closer to ω_* [Fig. 3(a)]. Using Eq. (4), we find the angle $\alpha_{\max}$ of the overall Cherenkov cone and the frequency ω_* at the cone:

$$\cot \alpha_{\max} = \frac{4\omega_{\mathrm{TO}}\omega_*(n_g^2-\varepsilon_\infty)^{1/2}}{\sqrt{3}n_g(\omega_{\mathrm{TO}}^2-\omega_*^2)}, \tag{30a}$$

$$\omega_* = \omega_{\mathrm{TO}}\sqrt{\sqrt{1+3(n_g^2-\varepsilon_0)/(n_g^2-\varepsilon_\infty)}-1}. \tag{30b}$$

In the superluminal regime, Eq. (29) has only one root ω_1 if $\varepsilon_\infty < n_g^2 < \varepsilon_0$. In this case, the maximum cone angle corresponds to zero frequency [Fig. 3(b)] and equals

$$\cot \alpha_{\max} = (\varepsilon_0/n_g^2-1)^{1/2}. \tag{31}$$

If $n_g^2 < \varepsilon_\infty$, the root ω_2 appears due to the upper branch of the dispersion curve. The maximum cone angle of the upper-branch polaritons corresponds to $\omega \to \infty$ [Fig. 3(b)] and equals

$$\cot \alpha_{\max} = (\varepsilon_\infty/n_g^2-1)^{1/2}. \tag{32}$$

In the strongly superluminal regime, when $\varepsilon_c(\omega)$ significantly exceeds n_g^2 and, therefore, can be approximated (at $\omega_{\mathrm{TO}}\tau_{\mathrm{FWHM}} \gg 1$) by ε_0, integral (27) can be evaluated analytically (see also Ref. 31):

$$E_y(z,x,t) = -\frac{2\pi^{3/2}p_y\ell_\perp\tau}{c\tau_{\mathrm{eff}}(\varepsilon_0-n_g^2)^{1/2}}\frac{d}{d\eta}F(\eta,\tau_{\mathrm{eff}}), \tag{33}$$

where $F(\eta,\tau_{\mathrm{eff}})$ is the Gaussian function (2) with $\eta=\xi-(|x|/c)(\varepsilon_0-n_g^2)^{1/2}$ used instead of ξ and $\tau_{\mathrm{eff}}=[\tau^2+\ell_\perp^2(\varepsilon_0-n_g^2)/c^2]^{1/2}$ used instead of τ. According to Eq. (33), the field distribution across the Cherenkov cone [Eq. (31)] is given by the derivative of the laser pulse intensity envelope taken with a negative sign, i.e., it consists of two adjacent terahertz pulses of opposite polarities. Interestingly, the effective characteristic time τ_{eff} of the Gaussian function $F(\eta,\tau_{\mathrm{eff}})$ and, therefore, the duration of the terahertz pulses at the Cherenkov cone (the cone's thickness), depends both on the duration τ and the transverse size $\ell_\perp$ of the optical pulse. For $\ell_\perp \gg c\tau(\varepsilon_0-n_g^2)^{-1/2}$, τ_{eff} depends mainly on $\ell_\perp$—the terahertz field distribution across the cone becomes smoother with increasing $\ell_\perp$. For $\ell_\perp \ll c\tau(\varepsilon_0-n_g^2)^{-1/2}$, τ_{eff} is practically independent of the degree of focusing and depends mainly on τ. According to Eq. (33), the maximum value of the terahertz field at the Cherenkov cone is

$$|E_y|_{\max} = \frac{(2\pi)^{3/2}p_y\ell_\perp\tau}{c\tau_{\mathrm{eff}}^2(\varepsilon_0-n_g^2)^{1/2}}e^{-1/2} \tag{34}$$

at $\eta=\pm\tau_{\mathrm{eff}}/\sqrt{2}$. For a fixed energy of the optical pulse, $p_y\ell_\perp\tau=$const in Eq. (34) and $|E_y|_{\max} \propto \tau_{\mathrm{eff}}^{-2}$. Thus, for a given τ, a decrease in $\ell_\perp$ leads to an increase in $|E_y|_{\max}$; however, when $\ell_\perp$ becomes smaller than $c\tau(\varepsilon_0-n_g^2)^{-1/2}$, further focusing adds little to the terahertz field magnitude. Similarly, for a given $\ell_\perp$, a decrease in τ leads to an increase in $|E_y|_{\max}$ until τ becomes smaller than $\ell_\perp(\varepsilon_0-n_g^2)^{1/2}/c$. If we fix the optical intensity rather than energy ($p_y=$const) and also fix $\ell_\perp$ in Eq. (34), then $|E_y|_{\max} \propto \tau/\tau_{\mathrm{eff}}^2$ and an optimal pulse duration $\tau_{\mathrm{opt}}=\ell_\perp(\varepsilon_0-n_g^2)^{1/2}/c$ appears that maximizes $|E_y|_{\max}$ to $(2/e)^{1/2}\pi^{3/2}p_y/(\varepsilon_0-n_g^2)$. Essentially, the generated terahertz spectrum $\propto p_y\ell_\perp\tau\omega\exp(-\omega^2\tau_{\mathrm{eff}}^2/4)$ [see Eq. (27)] has a maximum $\propto\tau_{\mathrm{eff}}^{-1}$ at $\omega\tau_{\mathrm{eff}}=\sqrt{2}$; the position and magnitude of the maximum depend on both parameters τ and $\ell_\perp$ of the laser pulse.

A weak absorption, described by Eq. (4) with $\gamma \ll \omega_{\mathrm{TO}}$, can be incorporated into Eq. (33) by substitution

$$\tau_{\mathrm{eff}} \to \left[\tau_{\mathrm{eff}}^2 + \frac{2\gamma(\varepsilon_0-\varepsilon_\infty)|x|}{\omega_{\mathrm{TO}}^2c(\varepsilon_0-n_g^2)^{1/2}}\right]^{1/2}. \tag{35}$$

According to Eqs. (33) and (35), absorption results in a gradual fading of the terahertz field at the Cherenkov cone and spreading of the field's distribution across the cone with distance $|x|$. Consequently, the Cherenkov cone acquires a finite size with a half-width estimated as

$$|x|_{\max} \sim \frac{\omega_{\mathrm{TO}}^2\tau_{\mathrm{eff}}^2c(\varepsilon_0-n_g^2)^{1/2}}{2\gamma(\varepsilon_0-\varepsilon_\infty)} \tag{36}$$

and the length $\Delta z=|x|_{\max}\cot\alpha_{\max}$.

Let us now proceed to the analysis of the optical-to-terahertz conversion in specific crystals using the general formulas we derived.

VI. TERAHERTZ GENERATION IN A SLAB: $LiNbO_3$, GaAs, AND ZnTe

To retrieve specific results from the general solution, we have to define dispersion and nonlinear properties of the material. Assuming that the material is undoped and, therefore, the contribution from free carriers can be neglected, we attribute the dispersion in the terahertz range to phonon resonances. We use mainly the one-resonance formula (4). However, in the case of ZnTe, a generalized formula including several phonon resonances will be used in the calculations for more accurate description of the linear absorption in the terahertz range.

According to our analysis, the component p_z of the nonlinear polarization generates terahertz radiation less efficiently as compared to $p_{x,y}$ and, in addition, it produces an inconvenient for practical applications angular distribution of terahertz emission from the slab with zero intensity in the z direction. Therefore, we focus on the crystallographic orientations of the materials that maximize p_x or p_y at $p_z=0$.

A. Strongly superluminal regime: $LiNbO_3$ excited with an 800 nm optical pump

To verify the correctness of our approach, we consider at first the emission of terahertz waves by Ti:sapphire laser pulses in a rather well studied superluminal material such as $LiNbO_3$. We compare our results with the calculations of Ref. 18 based on the dispersionless approximation of Ref. 31, two-dimensional finite-difference time-domain (FDTD) simulation of Ref. 41, and numerical and experimental results for $LiTaO_3$, which is another perovskite material similar to $LiNbO_3$.[6]

We consider the optimal geometry typically used in experiments: in our coordinate system, the optical axis of the crystal is along the y axis (Fig. 1), and the laser pulse is polarized along the optical axis and produces nonlinear polarization in the same direction with $p_y=d_{33}E_0^2$, where d_{33} is

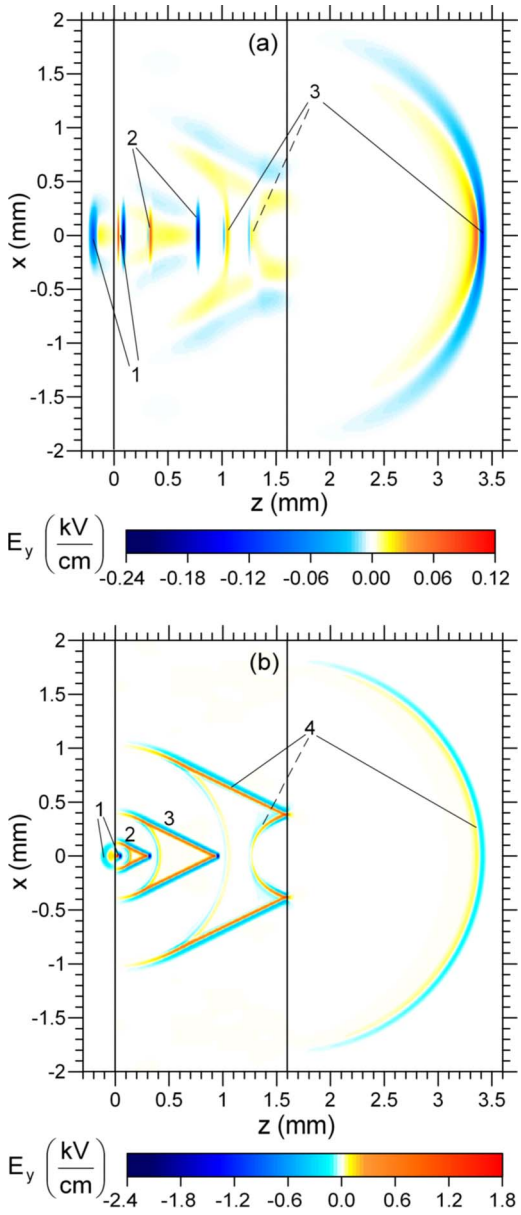

FIG. 4. (Color online) Snapshots of $E_y(z,x,t)$ in $LiNbO_3$ at successive moments of time (numerated in order) for (a) $\ell_{\perp \mathrm{FWHM}}=300\ \mu$m and (b) $\ell_{\perp \mathrm{FWHM}}=30\ \mu$m. The laser pulse duration is $\tau_{\mathrm{FWHM}}=150$ fs and the peak laser intensity I_0 is (a) 1 GW/cm^2 and (b) 10 GW/cm^2. The crystal thickness is $d=1.6$ mm, and the crystal boundaries are shown by the thin vertical lines. The dashed pointers show the terahertz fields reflected from the exit surface of the crystal.

the nonlinear coefficient and E_0 is the amplitude of the optical field in the crystal. Thus, only s-polarized terahertz waves will be generated by p_y. We used the one-phonon-resonance formula (4) with the same parameters as in Ref. 42: $\omega_{\mathrm{TO}}/(2\pi)=7.44$ THz, $\varepsilon_0=26$, $\varepsilon_\infty=10$, and $\gamma/(2\pi)=0.844$ THz. The optical group refractive index and nonlinear coefficient were taken from Ref. 9: $n_g=2.23$ and $d_{33}=166$ pm/V.[43] Since $n_g^2 \ll \varepsilon_0$, $LiNbO_3$ may be classified as a strongly superluminal material.

Figure 4 shows the spatial distribution of the electric field E_y calculated on the basis of Eqs. (10), (11), and (14) for

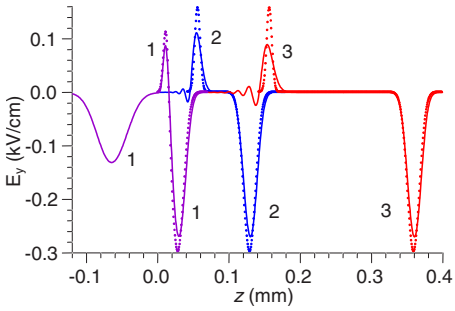

FIG. 5. (Color online) Snapshots of $E_y(z,t)$ in $LiNbO_3$ plotted on the basis of Eq. (18) (solid lines) and Eq. (19) (dashed lines) for successive moments of time (numerated in order). The laser pulse duration is $\tau_{\mathrm{FWHM}}=150$ fs and peak pulse intensity is $I_0=1$ GW/cm^2.

several successive moments of time and two values of the beam width $\ell_{\perp \mathrm{FWHM}}=300$ and 30 μm. In the calculations, the energy of the optical pulse (per unit length in the y direction) was fixed to 5 μJ/cm, so the peak laser intensity $I_0=(c/8\pi)n_{\mathrm{opt}}E_0^2$, with $n_{\mathrm{opt}}=2.16$ the optical refractive index,[9] differs by a factor of 10 in Figs. 4(a) and 4(b): 1 and 10 GW/cm^2, respectively. The laser pulse duration was $\tau_{\mathrm{FWHM}}=150$ fs, which is typical for experiments. This value is significantly smaller than $\ell_\perp(\varepsilon_0-n_g^2)^{1/2}/c$ in the formula for τ_{eff} at $\ell_{\perp \mathrm{FWHM}}=30\ \mu$m. For $LiNbO_3$, the inequality $\tau < \ell_\perp(\varepsilon_0-n_g^2)^{1/2}/c$ can be reduced to $\tau[\mathrm{fs}]<15\ell_\perp[\mu\mathrm{m}]$. Thus, using smaller τ_{FWHM} does not give any increase in the magnitude of the generated terahertz field according to discussion after Eq. (34).

In the case of weak focusing [Fig. 4(a)], the radiation pattern inside and near the crystal is practically one dimensional; weak rudiments of the Cherenkov cone are barely visible. On entering the crystal, the laser pulse produces reflected transient radiation in vacuum (moment 1). Inside the crystal, the pattern evolves in accord with Eq. (19) (moments 1 and 2). The two pulses (free and forced responses) have the same duration; their amplitudes differ by a factor of 2 and have opposite signs. They propagate with different velocities such that the free-wave response lags. The pulses become separated at the walk-off length $L_w^{\mathrm{space}} \approx 26\ \mu$m ($L_w \approx 16\ \mu$m). After that, the forced-wave pulse practically does not change; dispersion and absorption included in Fig. 4(a), but neglected in Eq. (19), lead to a gradual spreading and fading of the free-wave pulse as evident from a comparison between moments 2 and 3. At moment 3, we can also see the signals reflected from the exit surface of the crystal and transmitted through it. For the transmitted to vacuum radiation, one can see the formation of far field, which can be related to that in the near field by a temporal derivative[30] in agreement with Fig. 4(a).

To study more carefully the effects of dispersion and absorption, we compare the snapshots for $E_y(z,t)$ using the exact [Eq. (18)] and approximate [Eq. (19)] solutions in the one-dimensional case (Fig. 5). The agreement is very good for the forced-wave (negative) pulse, although Eq. (19) overestimates the pulse amplitude by $\sim 10\%$. For the free-wave response (positive pulse), the agreement is reasonable for z

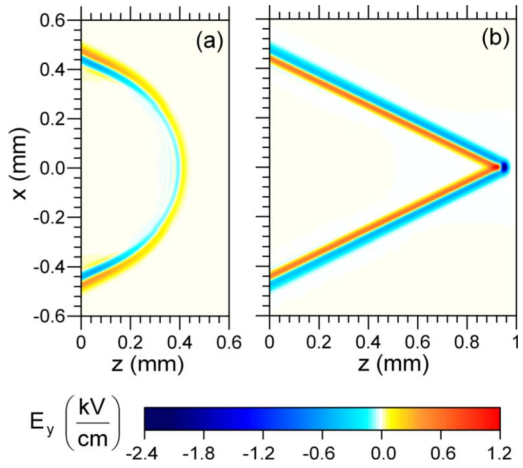

FIG. 6. (Color online) The (a) free-wave and (b) forced-wave responses in $LiNbO_3$ for the same parameters as in Fig. 4(b), moment 3.

~ 0.1 mm; for larger z, the dispersion broadening and absorption become significant. Calculations show that for longer optical pulses, the effect of dispersion manifests itself at larger z. Additionally, Fig. 5 demonstrates the growth of the positive pulse magnitude in the beginning of the generation process due to separation of the forced- and free-wave responses within the coherence length; simultaneously, the reflected terahertz pulse in the air is formed.

In the case of strong focusing [Fig. 4(b)], the radiation pattern produced by the laser pulse moving inside the crystal (the moments 1–3) consists of the Cherenkov cone (or wedge) with its apex on the moving laser pulse and a cylindrical wave propagating from the air-crystal interface $z=0$ in the $+z$ direction (there is also weak transient radiation in the air propagating in the opposite direction, shown for moment 1). These two main parts of the radiation pattern can be attributed, respectively, to the forced- and free-wave responses in Eq. (17). The free-wave response consists of the cylindrical and conical parts [Fig. 6(a)]; the conical part completely cancels the infinite Cherenkov cone of the forced-wave response [Fig. 6(b)] behind the points where the cone contacts the cylindrical wave [Fig. 4(b)]. Due to difference in optical and terahertz group refractive indices, the Cherenkov cone moves faster than the cylindrical wave in the $+z$ direction, whereas in the perpendicular to the cone's ray directions, they move synchronously and touch each other at all times [Fig. 4(b)]. The electric field at the cone varies in the normal to the cone direction as the first derivative of the laser pulse envelope, i.e., consists of two pulses of opposite polarities, according to Eq. (33). The opening angle of the Cherenkov cone $\alpha_{\max}$ is about 26°, in accord with Eq. (31). The Cherenkov angle $\theta_{ch}=\pi/2-\alpha_{\max}\approx 64°$ significantly exceeds the critical angle of the total internal reflection $\theta_{tot}\approx 11.3°$ at the crystal-air boundary. Consequently, the Cherenkov cone is totally internally reflected at the exit crystal-air interface [see Fig. 4(b), moment 4]. This agrees with predictions of Ref. 4. The cylindrical wave visible in the air at $z>d$ is the transient radiation propagating from the point where the laser pulse crosses the boundary $z=d$.

The radiation pattern for moments 2 and 3 in Fig. 4(b) is in good agreement with FDTD simulation of Ref. 41. Some discrepancy with Ref. 6 in the number of oscillations on the Cherenkov cone is due to the use of much shorter pulses (~ 60 fs) in Ref. 6 as compared to what we used for Fig. 4(b). The shorter pulses allowed the excitation of the upper branch of the phonon polariton dispersion curve. Moreover, damping was neglected in Ref. 6. Figure 4(b) also confirms the conclusion, made in Ref. 18, that the generated terahertz energy increases with the distance passed by the laser pulse in the crystal via increasing the size of the Cherenkov cone at constant terahertz intensity at the cone. The maximum size of the cone is, however, limited by Eq. (36) due to absorption in the terahertz range. For $\tau_{FWHM}=150$ fs and $\ell_{\perp FWHM}=30$ μm, the size of the Cherenkov cone in $LiNbO_3$ is estimated as $\Delta z\sim 4$ mm.

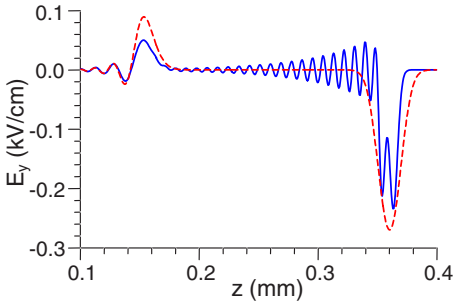

FIG. 7. (Color online) Snapshots of $E_y(z,t)$ in $LiNbO_3$ plotted on the basis of Eq. (18) for $\tau_{FWHM}=75$ fs (solid line) and $\tau_{FWHM}=150$ fs (dashed line). The peak laser intensity is $I_0=1$ GW/cm^2.

Figure 7, plotted on the basis of Eq. (18), demonstrates the effect of phase-matched excitation of the upper-branch phonon polaritons by a planar laser pulse shorter than 100 fs. Mathematically, the Gaussian factor $\tilde{F}(\omega)$ with $\tau_{FWHM}>100$ fs brings to naught the integrand in Eq. (18) at frequencies higher than $\omega_{LO}/(2\pi)\approx 12$ THz. The shorter laser pulses ($\tau_{FWHM}=75$ fs, Fig. 7) can excite the upper-branch polaritons much more efficiently and we clearly observe in Fig. 7 high-frequency oscillations imposed on the two-pulse structure formed by the lower-branch polaritons. Interestingly, absorption for the upper-branch polaritons decreases with its frequency. Consequently, polaritons with higher frequencies should reach higher magnitudes in the course of phase-matched excitation.

Finally, comparing the efficiencies of the optical-to-terahertz conversion in the cases of strong [Fig. 4(a)] and weak [Fig. 4(b)] focusing, one can see that the strong focusing allows one to generate much stronger terahertz fields inside the crystal. However, special efforts are required to extract the terahertz Cherenkov radiation from the crystal.[9,17–19] An interesting possibility is to generate p-polarized Cherenkov radiation and cut the crystal at the Brewster angle to the Cherenkov cone.

B. Weakly superluminal regime: GaAs excited with a 1.56 μm optical pump

In the case of GaAs excited with fiber laser pulses, we still have the superluminal regime but not so well pronounced as in $LiNbO_3$. Indeed, in GaAs the optical group

refractive index $n_g=3.55$ at 1.56 μm differs only slightly from $\sqrt{\varepsilon_0}=3.59$, where $\varepsilon_0=12.9$.[44] According to terminology of Sec. V, this case may be classified as the weakly superluminal regime.

We consider a ⟨110⟩-cut GaAs crystal with the [001] crystallographic axis oriented at an angle ≈55° with respect to the electric field of a linearly polarized laser beam. In this configuration (optimal for all zinc-blende crystals), the nonlinear polarization induced in the crystal due to optical rectification is maximal and codirectional with the electric field. The maximized amplitude of the nonlinear polarization is $p=\sqrt{4/3}d_{14}E_0^2$,[45] with $d_{14}=65.6$ pm/V the nonlinear coefficient.[9] We focus mainly on the case of s polarization, when $p=p_y$, although the peculiarities of terahertz emission from the slab in the case of p polarization, when $p=p_x$, will be discussed as well. We use the one-phonon-resonance formula (4) with $\omega_{TO}/(2\pi)=8.1$ THz, $\varepsilon_\infty=11$, and $\gamma/(2\pi)=0.07$ THz.[10]

Figure 8 shows the spatial distribution of the electric field E_y calculated on the basis of Eqs. (10), (11), and (14) for several successive moments of time and two values of the laser beam transverse size: $\ell_{\perp FWHM}=300$ and 30 μm. As before, the energy of the optical pulse is fixed (but now to 50 nJ/cm), so the peak laser intensity I_0 differs by a factor of 10 in Figs. 8(a) and 8(b): 10 and 100 MW/cm^2, respectively. The laser pulse duration is $\tau_{FWHM}=150$ fs.

In the case of weak focusing [Fig. 8(a)], the generated terahertz field evolves inside the crystal in accord with the scenario described in Sec. V for the weakly superluminal regime (moments 1–4): the free- and forced-wave responses practically cancel each other near the entrance surface $z=0$; the total terahertz field behaves, in general, according to Eq. (21), i.e., it follows the derivative of the optical intensity envelope and grows with z; multiple oscillations in the wave form (moments 3 and 4) arise due to dispersive distortion of the free-wave response. Incidence of the generated terahertz pulse on the exit surface of the crystal produces the reflected and transmitted terahertz radiations (moment 5); the transmitted to the air electric field is enhanced by a factor of ~1.6 due to reduction in the refractive index. The output radiation contains more oscillations in the far field (moment 5) as compared to the case of $LiNbO_3$. It is noteworthy that the reflected transient radiation in the air ($z<0$) is indiscernible in Fig. 8(a) (moment 1) because of its weakness in comparison with the output terahertz radiation.

To illustrate the dynamics of the terahertz field generation inside the crystal in more detail, we plotted in Fig. 9 the forced- and free-wave responses, as well as the total terahertz field, calculated for several successive moments of time using the one-dimensional Eq. (18). It is seen in Fig. 9 that the dispersionless approximation (21) works very well up to z ~1 mm; for larger z, an essential oscillatory tail forms in the wave form due to dispersion. The walk-off length L_w, introduced in Sec. V and taken at $n_t=\sqrt{\varepsilon_0}$, is estimated for $\tau_{FWHM}=150$ fs and parameters of GaAs as $L_w \approx L_w^{space}$ ~1.1 mm. At this distance, the forced- and free-wave responses become separated at the half-amplitude level.

In the case of strong focusing [Fig. 8(b)], the general structure of the radiation pattern formed behind the moving source (moments 1–4) is similar to that for $LiNbO_3$: the forward part is the Cherenkov cone of the forced-wave response which is followed by the cylindrical wave of the free-wave response. The opening angle of the Cherenkov cone is about 81° that is in accord with Eq. (31). As in $LiNbO_3$, the conical part of the free-wave response [Fig. 10(a)] cancels the Cherenkov cone [Fig. 10(b)] behind the points where the cylindrical wave touches the Cherenkov cone [Fig. 10(c)]. Due to proximity of the velocities of the Cherenkov cone and the cylindrical wave in GaAs, they are not so well separated as in $LiNbO_3$ at distances $z \leqslant 1$ mm that are typically used in experiments.[10] Nevertheless, the total terahertz field generated at such distances is only an order of magnitude smaller than in $LiNbO_3$ even for optical intensities which are 100 times lower [compare with Fig. 4(b)]. Additionally, dispersion gives rise to several oscillations both on the Cherenkov

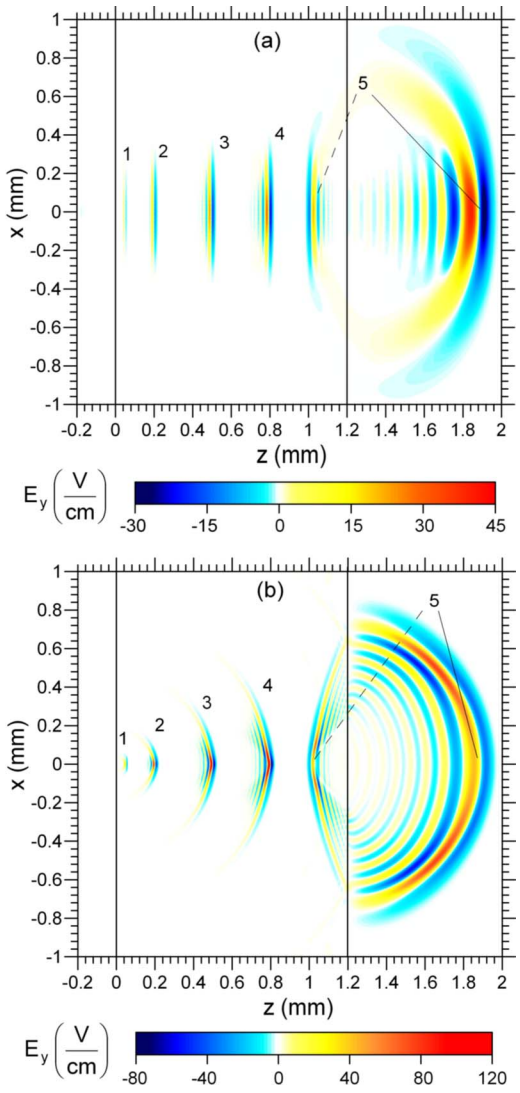

FIG. 8. (Color online) Snapshots of $E_y(z,x,t)$ in GaAs at successive moments of time (numerated in order) for (a) $\ell_{\perp FWHM}=300$ μm and (b) $\ell_{\perp FWHM}=30$ μm. The laser pulse duration is $\tau_{FWHM}=150$ fs and peak laser intensity I_0 is (a) 10 MW/cm^2 and (b) 100 MW/cm^2. The crystal thickness is $d=1.2$ mm, and the crystal boundaries are shown by the thin vertical lines. The dashed pointers show the terahertz fields reflected from the exit surface of the crystal.

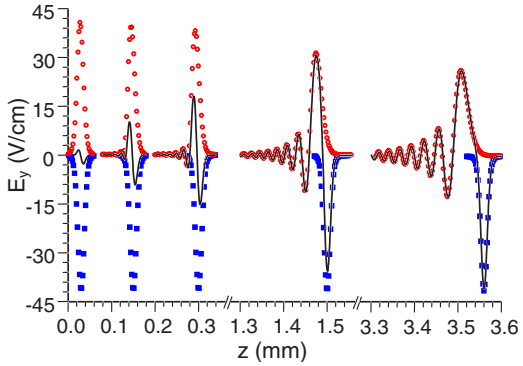

FIG. 9. (Color online) The free-wave (open circle) and forced-wave (filled square) responses and the total terahertz field $E_y(z,t)$ (solid line) in GaAs plotted on the basis of Eq. (18) for successive moments of time. The laser pulse duration is $\tau_{\mathrm{FWHM}}=150$ fs and peak laser intensity is $I_0=10$ MW/cm^2.

cone and free-wave response [Figs. 10(a) and 10(b)]; in the course of propagation, the free-wave response spreads in the number of oscillations. Since the Cherenkov angle $\theta_{\mathrm{ch}}=\pi/2-\alpha_{\max}\approx 9°$ is less than the critical angle of the total internal reflection $\theta_{\mathrm{tot}}\approx 16.2°$ at the crystal-air boundary, the Cherenkov cone couples to outgoing radiation in vacuum [moment 5 in Fig. 8(b), the reflected to the crystal radiation at this moment is also seen in Fig. 8(b)].

For practice, it is interesting to study the dependence of the optical-to-terahertz conversion efficiency on the degree of the optical focusing and the crystal thickness. Figure 11 shows the conversion efficiency as a function of $\ell_{\perp\mathrm{FWHM}}$ for two polarizations of the optical pump and two crystal thicknesses. The generated terahertz energy was calculated using the time window to filter out the rereflected terahertz pulses

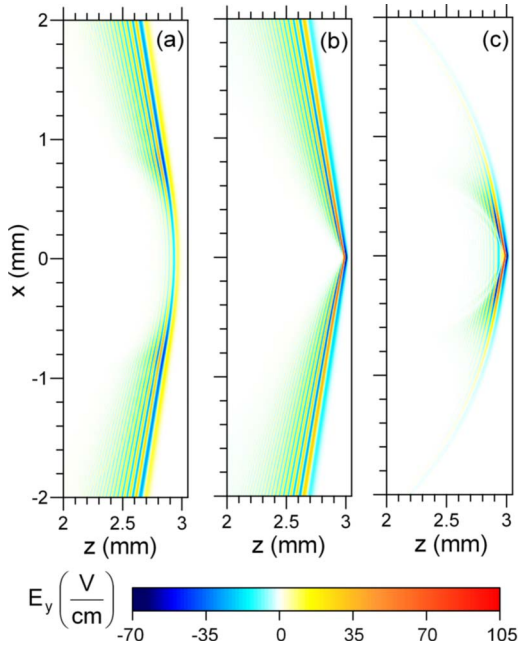

FIG. 10. (Color online) The (a) free-wave and (b) forced-wave responses and (c) the total terahertz field in GaAs for the same parameters as in Fig. 8(b).

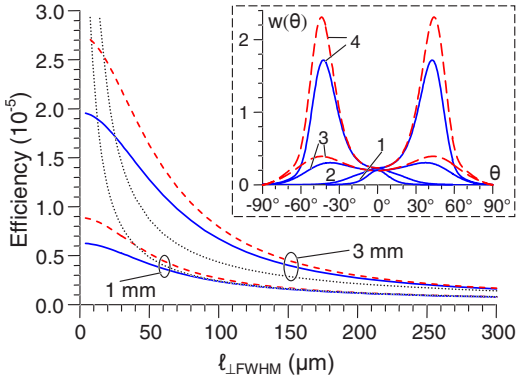

FIG. 11. (Color online) Efficiency of the optical-to-terahertz conversion in a slab of GaAs as a function of the laser width $\ell_{\perp\mathrm{FWHM}}$ for s (solid line) and p polarization (dashed line) of the optical pump and two thicknesses of the slab (values shown near corresponding curves). Dotted curves show the result of calculation in the plane-wave approximation. The laser energy is fixed and corresponds to intensity $I_0=10$ MW/cm^2 at $\ell_{\perp\mathrm{FWHM}}=300$ μm, laser pulse duration $\tau_{\mathrm{FWHM}}=150$ fs. Inset: Angular density of the terahertz energy emitted from the slab for s (solid line) and p polarization (dashed line): (1) $\ell_{\perp\mathrm{FWHM}}=300$ μm and $d=1$ mm, (2) $\ell_{\perp\mathrm{FWHM}}=300$ μm and $d=3$ mm, (3) $\ell_{\perp\mathrm{FWHM}}=30$ μm and $d=1$ mm, and (4) $\ell_{\perp\mathrm{FWHM}}=30$ μm and $d=3$ mm. For (1) and (2), the curves for s and p polarizations coincide.

(see Sec. IV). Three conclusions can be drawn from Fig. 11. First, the applicability of the plane-wave approximation depends on the crystal thickness: with increasing d, this approximation becomes unsatisfactory at greater $\ell_{\perp\mathrm{FWHM}}$. If we plot the efficiency as a function of the crystal thickness calculated using the plane-wave approximation, it has a maximum at $d\approx 2$ mm. The maximum results from the interplay of two factors—the growth of the total terahertz field with z (within the walk-off length L_w) due to separation of the forced- and free-wave responses and weak gradual damping with z of the free-wave response. At the same time, for a wide pulse (but of finite $\ell_{\perp\mathrm{FWHM}}$, for example, 300 μm), the conversion efficiency increases monotonically with d. This can be attributed to the generation of obliquely propagating plane waves by the edges of the laser pulse; correspondingly, the angular spectrum of the generated terahertz radiation widens with d (see curves 1 and 2 in the inset of Fig. 11). Second, for strongly focused optical pump ($\ell_{\perp\mathrm{FWHM}}\leqslant 50$ μm), the efficiency is appreciably higher for p than for s polarization of the pump owing to higher transmission of p-polarized terahertz waves to vacuum. Third, the efficiency growth with the crystal thickness d is more pronounced for strongly focused laser pulses. For such pulses, the generated terahertz energy grows with the propagation distance due to lengthening of the Cherenkov cone; this is clearly demonstrated by forming peaks in the generated angular spectrum (curves 3 and 4 in the inset of Fig. 11). The presence of the peaks in the spectrum corresponds to the formation of a hollow terahertz beam in the far-field region.

Figure 12 shows the spectral-angular density of the radiated energy $w_s(\theta,\omega)$ [Eq. (16) with $C_4(g,\omega)$ convoluted with the Fourier spectrum of the time window] for $d=3$ mm and two values of the beam transverse size: $\ell_{\perp\mathrm{FWHM}}=300$ and

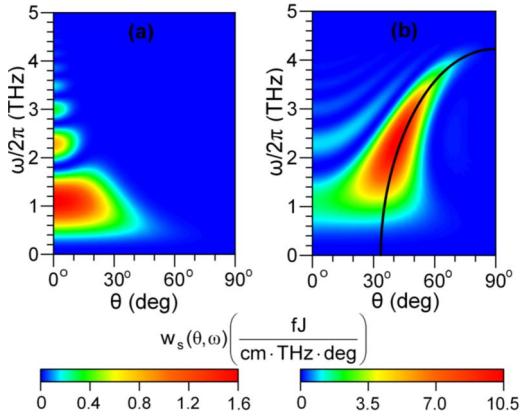

FIG. 12. (Color online) Spectral-angular density of terahertz energy emitted from a slab of GaAs for (a) $\ell_{\perp \mathrm{FWHM}}=300\ \mu$m, $I_0=10\ \mathrm{MW/cm^2}$ and (b) $\ell_{\perp \mathrm{FWHM}}=30\ \mu$m, $I_0=100\ \mathrm{MW/cm^2}$. The optical pulse is s polarized and its duration is $\tau_{\mathrm{FWHM}}=150$ fs. The solid line in (b) shows the relation between the emission angle and frequency calculated using the Cherenkov condition $\sin\alpha=n_g/\sqrt{\varepsilon_c(\omega)}$ and Snell's law.

30 μm. For the weakly focused laser pulse ($\ell_{\perp \mathrm{FWHM}}=300\ \mu$m), the generated terahertz energy is predominantly distributed in a comparatively narrow frequency interval around 1 THz [0.8 THz$\leqslant\omega/(2\pi)\leqslant$1.3 THz] and over small angles $\theta\leqslant 15°$. For the strongly focused laser pulse ($\ell_{\perp \mathrm{FWHM}}=30\ \mu$m), the energy is distributed over higher frequencies [1.5 THz$\leqslant\omega/(2\pi)\leqslant$3 THz] and higher angles ($30°\leqslant\theta\leqslant 50°$). The maximum of the spectral-angular density lies on the curve described by Cherenkov condition $\sin\alpha=n_g/\sqrt{\varepsilon_c(\omega)}$ in which the angle α is related to the emission angle in vacuum θ by Snell's law (solid line in Fig. 12). Comparing frames (a) and (b) in Fig. 12, one can conclude that the emitted terahertz spectrum can be controlled by varying the transverse size of the laser beam.

Our results were obtained under the assumption that the diffractive and dispersive broadening of the laser pulse is negligible. In practice, these factors put limits on the increase of the crystal thickness and on the decrease of the pulse's width and duration. In Fig. 13, we plotted the conversion efficiency as a function of the crystal thickness d choosing $\ell_\perp$ for every d from the condition that the Rayleigh length $2\pi n_{\mathrm{opt}}\ell_\perp^2/\lambda$ ($\lambda=1.56\ \mu$m, $n_{\mathrm{opt}}=3.38$ optical refractive index[44]) equals d, i.e., choosing the minimal possible $\ell_\perp$ admitted by diffraction. The dashed segment of the curve shows the region where d is greater than the length of dispersion broadening of the optical pulse $L_{\mathrm{disp}}=\tau^2/|\partial^2 k_{\mathrm{opt}}/\partial\omega^2|$, with k_{opt} the optical wave vector. In the dashed region, the dispersion broadening is significant for $\tau_{\mathrm{FWHM}}=150$ fs. It follows from Fig. 13 that there is an optimal thickness $d\sim 3-10$ cm where the efficiency is maximal. However, for so large thicknesses, dispersion broadening is significant. Thus, to maximize the efficiency, one should take the maximal possible thickness $d\sim 1$ cm, that is admitted by the dispersion, and focus the beam to the minimal size $\ell_{\perp \mathrm{FWHM}}\sim 30-50\ \mu$m for which the diffractive broadening is still not crucial (Fig. 13). The maximal efficiency is $\sim 3\times 10^{-5}$.

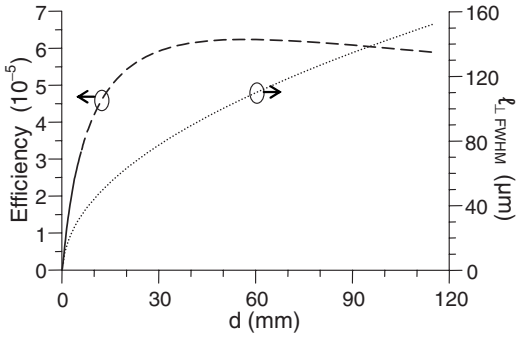

FIG. 13. Efficiency of the optical-to-terahertz conversion in a slab of GaAs as a function of slab thickness d (solid-dashed line) for the laser beam width $\ell_{\perp \mathrm{FWHM}}$ (dotted line) calculated from the condition that the Rayleigh length equals d. The dashed segment shows the region of thicknesses where dispersion broadening of the optical pulse is significant. The optical pump is s polarized, the laser energy is fixed at 50 nJ/cm, and $\tau_{\mathrm{FWHM}}=150$ fs.

C. Subluminal regime: ZnTe excited with a 780 nm optical pump

Let us now consider the subluminal regime of terahertz generation in a slab of ZnTe excited with a Ti:sapphire laser pulse. We take a ⟨110⟩-cut ZnTe crystal typically used in experiments. The crystal orientation is the same as for GaAs (see Sec. VI B). The nonlinear coefficient d_{14} in the formula for the nonlinear polarization (Sec. VI B) is taken equal to 68 pm/V.[9] The optical group refractive index is $n_g=3.28$ at 780 nm.[20] We use two models for the dielectric permittivity of ZnTe. In the first (simple) model, we take Eq. (4) with the following parameters: $\varepsilon_0=10$, $\varepsilon_\infty=7.44$, $\omega_{\mathrm{TO}}/(2\pi)=5.32$ THz, and $\gamma/(2\pi)=0.005$ THz. The small value of the damping rate γ is used to not obscure the qualitative features of the terahertz field dynamics and, at the same time, to avoid peculiarities in Fourier integrals [Eqs. (14) and (17)] at $\gamma=0$. However, the experimentally measured absorption spectrum of ZnTe below 5 THz has a behavior that is more complicated than described by the one-resonance approximation.[22,24,39,40] To model it accurately, we add three analogous terms to the simple model and fit the resonance frequencies, damping rates, and oscillator strengths of all four terms, as well as ε_∞, to the experimental data of Refs. 22, 24, 39, and 40.

Figure 14 shows the spatial distribution of the electric field E_y calculated on the basis of Eqs. (10), (11), and (14) for several successive moments of time and two values of the laser beam transverse size: $\ell_{\perp \mathrm{FWHM}}=300$ and 30 μm. The energy of the optical pulse is fixed (50 nJ/cm), so the peak laser intensity I_0 differs by a factor of 10 in Figs. 14(a) and 14(b): 10 and 100 $\mathrm{MW/cm^2}$, respectively. The laser pulse duration is $\tau_{\mathrm{FWHM}}=150$ fs. We used the four-resonance model of dispersion and absorption in the calculations.

In the case of weak focusing [Fig. 14(a)], the generated terahertz field in ZnTe resembles the one for GaAs (see Sec. VI B). The only noticeable difference is the appearance of weak oscillations running in front of the main pulse. These oscillations, which propagate faster than the optical pulse, are the phonon polaritons that lie below the intersection point

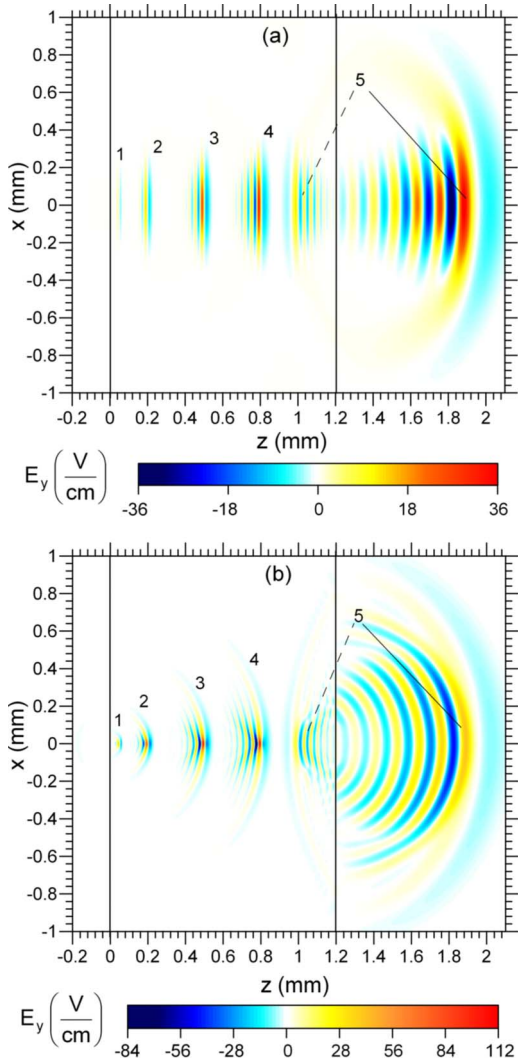

FIG. 14. (Color online) Snapshots of $E_y(z,x,t)$ in ZnTe at successive moments of time for (a) $\ell_{\perp \mathrm{FWHM}}=300\ \mu$m and (b) $\ell_{\perp \mathrm{FWHM}}=30\ \mu$m. The laser pulse duration is $\tau_{\mathrm{FWHM}}=150$ fs and the peak laser intensity I_0 is (a) 10 MW/cm^2 and (b) 100 MW/cm^2. The crystal thickness is $d=1.2$ mm, and the crystal boundaries are shown by the thin vertical lines. The dashed pointers show the terahertz fields reflected from the exit surface of the crystal.

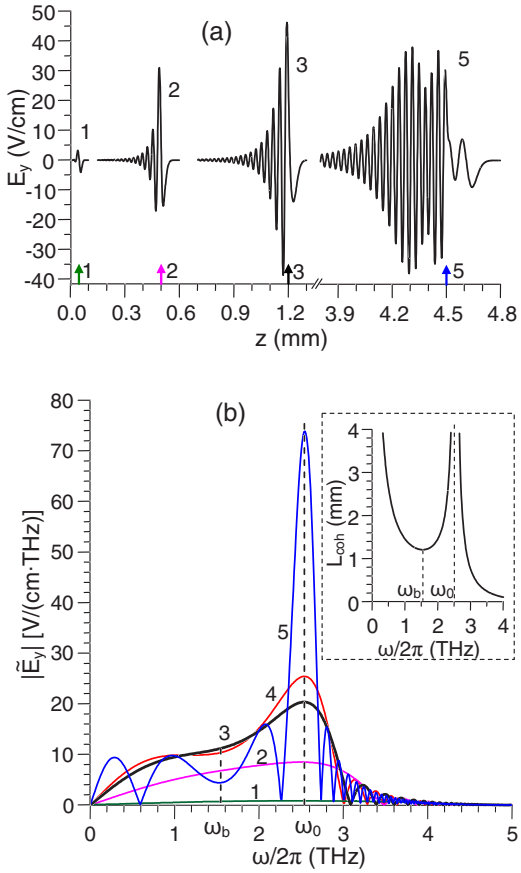

FIG. 15. (Color online) (a) Snapshots of $E_y(z)$ in ZnTe at successive moments of time for $\tau_{\mathrm{FWHM}}=150$ fs and $I_0=10$ MW/cm^2 in the 1D case. (b) Spectra of $E_y(z)$ at several points along z [labeled by arrows on (a), curve 4 is for $z=1.5$ mm] for the same parameters as in (a). The inset in (b) shows the conventional coherence length $L_{\mathrm{coh}}(\omega)$ given by Eq. (38) as a function of terahertz frequency. The frequency ω_b defines the minimal $L_{\mathrm{coh}}(\omega)$, and ω_0 is the frequency where phase matching occurs.

of their low-frequency dispersion branch and the line $k=\omega/V$ (see Fig. 2). The oscillations are a part of the free-wave response transiently excited at the interface $z=0$.

To illustrate the field dynamics in ZnTe in more detail, we study the one-dimensional model (see Fig. 15, the one-resonance model of absorption is used). The formation of the terahertz pulse can be divided into two stages. During the first stage, the pulse grows in magnitude without significant changes in its shape [see moments labeled as 1, 2, and 3 in Fig. 15(a)]. During the second stage, the pulse grows in length without significant change in amplitude [see moment 5 in Fig. 15(a)]. To define the length at which the transition from stage 1 to stage 2 takes place, we plot the field spectra in Fig. 15(b) at several points along z. For $z<1.2$ mm, the main part of the spectrum grows with z. This means that the pulse also grows as it propagates without changing its shape.

After $z=1.2$ mm, a part of the spectrum in the vicinity of a certain frequency ω_b starts to decrease with z, whereas other frequencies continue to grow [most rapidly in the vicinity of the frequency ω_0 for which the phase matching occurs, see Fig. 15(b)]. Correspondingly, the pulse shape should deform too. One can define the distance when this starts to occur as the buildup length. Mathematically, the buildup length is the minimal distance at which a frequency component of $|\tilde{E}_y(\omega,z)|$ reaches maximum. This is equivalent to solving

$$\frac{\partial|\tilde{E}_z(\omega,z)|}{\partial z}=0. \tag{37}$$

Solving Eq. (37) gives the dependence $z(\omega)$, which describes the positions inside crystal where various field components reach their maxima. Using this dependence, we can find the frequency ω_b that gives the minimal z and define corresponding buildup length $L_b=z(\omega_b)$. Substituting Eq. (18) into Eq. (37), we obtain

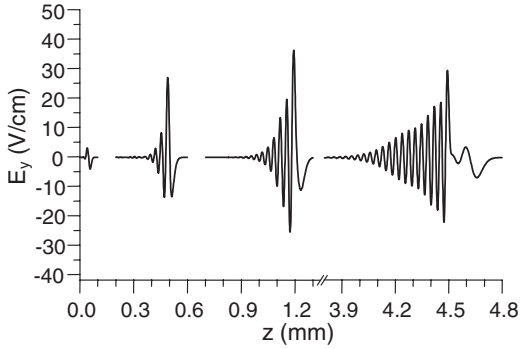

FIG. 16. Snapshots of $E_y(z)$ in ZnTe for the same moments of time and same parameters as in Fig. 15 but for more realistic four-resonance model of absorption.

$$z(\omega) = \frac{c\pi}{\omega|\sqrt{\varepsilon_c(\omega)} - n_g|}. \tag{38}$$

This equation describes the so-called coherence length $z(\omega) = L_{\text{coh}}(\omega)$.[20] Thus, when phase matching occurs, the buildup length is the minimum of $L_{\text{coh}}(\omega)$: $L_b = \min L_{\text{coh}}(\omega) = L_{\text{coh}}(\omega_b)$ [inset of Fig. 15(b)].

Calculations using more realistic four-resonance model of terahertz absorption in ZnTe do not give a significant difference from the above considered two-stage dynamics of terahertz generation (Fig. 16). The stronger absorption influences mainly the limiting form of the terahertz field at large z. This form is in accord with Eq. (24) where γ is defined from the experimental data of Refs. 22, 24, 39, and 40 on the terahertz absorption at the phase-matched frequency ω_0.

The formation dynamics of the terahertz signal in ZnTe, which we just described, clearly shows that the similarity between the generated terahertz signals in GaAs and ZnTe, which is observed in Figs. 8(a) and 14(a), can be rather misleading as the signals are generated by two different physical mechanisms. In the case of GaAs, the terahertz signal (free-wave term) will always lag behind the generating optical pulse for sufficiently long crystals, longer than the walk-off length. While the terahertz pulse propagates, it spreads due to dispersion; it also becomes weaker due to absorption. For long samples, it completely disappears. This pulse is the transient solution generated only because of the presence of the boundary. In contrast, in ZnTe the terahertz signal never lags behind the optical pulse but only becomes longer with time. For infinitely long sample, the length of the terahertz pulse is determined by absorption. This pulse is the forced-wave solution. Thus, the similarity of patterns in Figs. 8(a) and 14(a) can be attributed to rather small slab thicknesses and importance of transient response in calculating the terahertz signal.

In the case of strong focusing [Fig. 14(b)], one can discern the following components in the radiation pattern: a cone, cylindrical waves outside the cone, and a plane wave propagating in the z direction inside the cone. To interpret the pattern, we plotted separately the free-wave [Fig. 17(a)] and forced-wave [Fig. 17(b)] responses, as well as the total terahertz field [Fig. 17(c)], for a large distance $z \sim 3$ mm

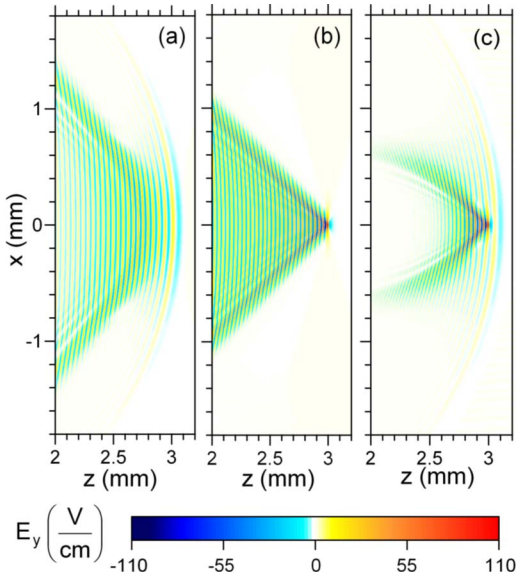

FIG. 17. (Color online) The (a) free-wave and (b) forced-wave responses and (c) the total terahertz field in ZnTe for the same parameters as in Fig. 14(b).

where all components of the pattern are more pronounced (the one-resonance model with small absorption was used). The forced-wave response consists of the Cherenkov cone and the plane wave. The cone has angle $\alpha_{\max} \approx 45°$ and frequency ω_* given by Eqs. (30a) and (30b). The plane wave is excited owing to phase matching and has frequency ω_0 given by Eq. (23). The beatings in the field distribution that are visible in Fig. 17(b) near the cone are explained by Eq. (28) and Fig. 3. Unlike the cases of $LiNbO_3$ and GaAs, the wave fronts at the cone are tilted at a large angle to the cone and propagate almost along the z axis—at an angle $\approx 10°$ to the axis as can be found from Eq. (28). Interestingly, the structure of the cone is similar to that predicted in Ref. 46 for the Cherenkov radiation from a laser pulse propagating through a magnetoplasma. The free-wave response has a more complicated structure [Fig. 17(a)] and is formed by the waves that belong to different segments of the dispersion curve—the fast waves with $0 < \omega < \omega_0$, the phase-matched wave at ω_0, and the slow waves with $\omega_0 < \omega < \omega_{\text{TO}}$. Note that the low-frequency oscillations have velocities greater than c/n_g and thus run in front of the main pulse. Despite the complicated structure of the total terahertz field [Fig. 17(c)], the propagation directions of the wave fronts do not deviate significantly from the z axis almost in all points of the radiation pattern. As a result, the maximum of terahertz emission from the slab is in the forward direction [Fig. 14(b)]. This differs drastically from the case of GaAs where the radiation pattern inside the slab, which is quite similar to that in ZnTe at a first glance, forms a hollow beam structure outside the slab [Fig. 8(b)].

Figure 18 shows the conversion efficiency as a function of $\ell_{\perp \text{FWHM}}$ for two polarizations of the optical pump and three crystal thicknesses. Five conclusions can be drawn from Fig. 18. First, although the efficiency increases with the crystal thickness, it saturates at $d \approx 3$ mm. Calculations for $d > 3$ mm show that the efficiency practically does not in-

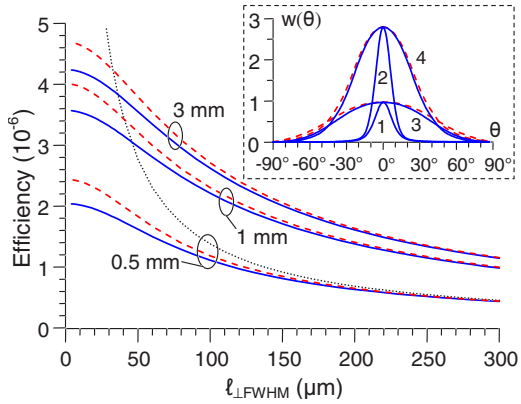

FIG. 18. (Color online) Efficiency of the optical-to-terahertz conversion in a slab of ZnTe as a function of the laser width $\ell_{\perp FWHM}$ for s (solid line) and p polarization (dashed line) of the optical pump and three thicknesses of the slab (values shown near corresponding curves). The dotted curve shows the result of calculation in the plane-wave approximation for $d=0.5$ mm. The laser energy is fixed and corresponds to intensity $I_0=10$ MW/cm^2 at $\ell_{\perp FWHM}=300$ μm, and the laser pulse duration is $\tau_{FWHM}=150$ fs. Inset: Angular density of the terahertz energy emitted from the slab for s (solid line) and p polarization (dashed line): (1) $\ell_{\perp FWHM}=300$ μm and $d=0.5$ mm, (2) $\ell_{\perp FWHM}=300$ μm and $d=3$ mm, (3) $\ell_{\perp FWHM}=30$ μm and $d=0.5$ mm, and (4) $\ell_{\perp FWHM}=30$ μm and $d=3$ mm. For (1) and (2), the curves for s and p polarizations coincide.

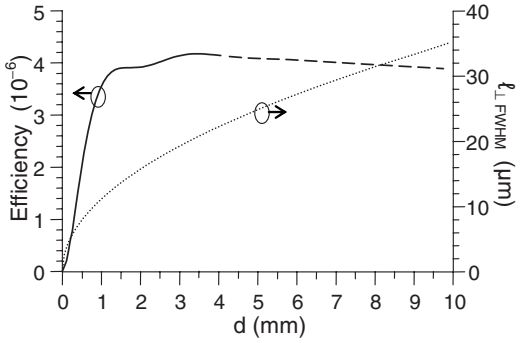

FIG. 19. Efficiency of the optical-to-terahertz conversion in a slab of ZnTe as a function of slab thickness d (solid-dashed line) for the laser beam width $\ell_{\perp FWHM}$ (dotted line) calculated from the condition that the Rayleigh length equals d. The dashed segment shows the region of thicknesses where dispersion broadening is significant. The optical pump is s polarized, laser energy is fixed to 50 nJ/cm, and $\tau_{FWHM}=150$ fs.

crease anymore. Thus, in practice it is useless to take crystals thicker than ~3 mm. Second, the maximum of the angular spectrum lies at $\theta=0$ independent of the crystal thickness and the laser beam width (inset of Fig. 18), unlike the case of GaAs. This confirms the conclusion of the previous paragraph about the relation of the direction of terahertz emission from the slab with the structure of the terahertz field inside the slab. Third, maxima of the angular spectra for different $\ell_{\perp FWHM}$ coincide (inset of Fig. 18). The increase of the efficiency with focusing is due to widening of the angular spectrum. Fourth, the angular spectrum is more narrow for thicker crystals. It can be explained by the lengthening of the Cherenkov cone and the plane wave inside the cone [compare Figs. 14(b) and 17(c)]. Fifth, the efficiency is almost an order of magnitude smaller than the one for the GaAs crystal of the same thickness and the same energy of the pump laser pulse (compare with Fig. 11).

To study the limitations imposed on the achievable efficiency by the diffractive and dispersive broadening of the laser pulse, we plotted in Fig. 19 the efficiency as a function of the crystal thickness d. As for GaAs (see discussion of Fig. 13 in Sec. VI B), we determined $\ell_{\perp}$ using the condition that the Rayleigh length [taken at $\lambda=780$ nm and $n_{opt}=2.86$ (Ref. 10)] equals d. It follows from Fig. 19 that the optimal thickness is $d\sim 1-3$ mm and corresponding values of the laser width are $\ell_{\perp FWHM}\sim 10-20$ μm. The maximal efficiency is $\sim 4\times 10^{-6}$.

VII. CONCLUSION

To conclude, we have developed a theory that describes terahertz generation via optical rectification of femtosecond laser pulses in a slab of an electro-optic material in the case when the pulse is focused to a line. Particular emphasis was made on the formation of the terahertz signal upon the entrance of the optical pulse into the crystal and its subsequent reshaping during the course of propagation. To relate our results to possible comparison with experiments, we also accounted for the transmission of the terahertz signal into vacuum. The general formulas that we obtained include the pulse parameters (width, duration, its group velocity) as well as the material properties (dispersion and absorption of terahertz waves in the crystal). Using the formulas, we studied two situations of practical interest: when the optical group velocity is greater than the fastest phase velocity of the copropagating terahertz waves (superluminal regime) and when it is smaller (subluminal regime).

In the case of superluminal excitation, the resultant terahertz field can be represented as a superposition of two terahertz pulses (free and forced responses) that are formed upon the entrance of the optical pulse into the slab. Initially, the pulses overlap but become separated with propagation distance due to difference in their velocities. Using our formalism, we rigorously defined a walk-off length as the distance at which the pulses become separated in time. This quantity, which has a clear physical meaning, is an adequate characteristic of the terahertz generation process. Our theory also predicted the formation of a backward propagating terahertz pulse in vacuum after the optical pulse enters the crystal. This prediction resulted from our use of the correct boundary condition for the terahertz field (i.e., continuity of the field), in contrast to the commonly assumed vanishing value of the field.

In the case of subluminal excitation, one can also separate the field into free and forced terms. However, due to phase matching, these terms do not become separated in space. It is more convenient to separate dynamics into two stages of field formation. In the first stage, the terahertz pulse grows in magnitude, while in the second it grows in length. We defined the buildup distance that separates the two stages.

Both in the superluminal and subluminal regimes, our theory gives a coherent consideration of the generated tera-

hertz energy in dependence on laser focusing, in contrast to the plane-wave approximation and models based on Bethe's diffraction theory.[22,26]

Finally, we would like to finish our analysis with specific recommendations on how to achieve efficient terahertz generation in various regimes in common materials such as ZnTe and GaAs.

(1) In the case of ZnTe illuminated with ~800 nm femtosecond laser pulses, the crystal thickness should be chosen in the interval of 1–3 mm and the laser beam should be focused to a width of 10–20 μm.

(2) In the case of GaAs illuminated with ~1.5 μm laser pulses, the crystal thickness should be taken as large as it admitted by the dispersion broadening of the laser pulse, i.e., about 1 cm for 100–200 fs pulses. The laser beam should be focused to 30–40 μm.

The recommendations are applicable to intensities lower than 100 MW/cm^2 for which two-photon absorption of the optical pump is negligible.

ACKNOWLEDGMENTS

Two of the authors (M.I.B. and S.B.B.) were supported in part by RFBR Grants Nos. 05-02-39022 and 06-02-17495. S.B.B. also acknowledges partial support from the fund "Dynasty." Another author (A.V.M.) was supported in part by NASA grant to ELORET Corporation (Sunnyvale, California). Part of this work has been supported by the Grant-in-Aid for Scientific Research from the Japanese Society of Promotion of Science.

*Present address: Canon Development Americas, Inc., Irvine, CA.

[1] T. Yajima and N. Takeuchi, Jpn. J. Appl. Phys. **9**, 1361 (1970).
[2] K. H. Yang, P. L. Richards, and Y. R. Shen, Appl. Phys. Lett. **19**, 320 (1971).
[3] D. H. Auston, K. P. Cheung, J. A. Valdmanis, and D. A. Kleinman, Phys. Rev. Lett. **53**, 1555 (1984).
[4] B. B. Hu, X.-C. Zhang, D. H. Auston, and P. R. Smith, Appl. Phys. Lett. **56**, 506 (1990).
[5] T. E. Stevens, J. K. Wahlstrand, J. Kuhl, and R. Merlin, Science **291**, 627 (2001).
[6] J. K. Wahlstrand and R. Merlin, Phys. Rev. B **68**, 054301 (2003).
[7] G. A. Askar'yan, Zh. Eksp. Teor. Fiz. **42**, 1360 (1962) [Sov. Phys. JETP **15**, 943 (1962)]; Phys. Rev. Lett. **57**, 2470 (1986).
[8] L. Xu, X.-C. Zhang, and D. H. Auston, Appl. Phys. Lett. **61**, 1784 (1992).
[9] J. Hebling, A. G. Stepanov, G. Almasi, B. Bartal, and J. Kuhl, Appl. Phys. B: Lasers Opt. **78**, 593 (2004).
[10] M. Nagai, K. Tanaka, H. Ohtake, T. Bessho, T. Sgiura, T. Hirosumi, and M. Yoshida, Appl. Phys. Lett. **85**, 3974 (2004).
[11] K. L. Vodopyanov, Opt. Express **14**, 2263 (2006).
[12] Y.-S. Lee, T. Meade, V. Perlin, H. Winful, T. B. Norris, and A. Galvanauskas, Appl. Phys. Lett. **76**, 2505 (2000).
[13] Y.-S. Lee, T. Meade, M. DeCamp, H. Winful, T. B. Norris, and A. Galvanauskas, Appl. Phys. Lett. **77**, 1244 (2000).
[14] G. Imeshev, M. E. Fermann, K. L. Vodopyanov, M. M. Fejer, X. Yu, J. S. Harris, D. Bliss, and C. Lynch, Opt. Express **14**, 4439 (2006).
[15] Y.-S. Lee, W. C. Hurlbut, K. L. Vodopyanov, M. M. Fejer, and V. G. Kozlov, Appl. Phys. Lett. **89**, 181104 (2006).
[16] J. Hebling, G. Almasi, I. Kozma, and J. Kuhl, Opt. Express **10**, 1161 (2002).
[17] A. G. Stepanov, J. Hebling, and J. Kuhl, Appl. Phys. Lett. **83**, 3000 (2003).
[18] A. G. Stepanov, J. Kuhl, I. Z. Kozma, E. Riedle, G. Almasi, and J. Hebling, Opt. Express **13**, 5762 (2005).
[19] M. Theuer, G. Torosyan, C. Rau, R. Beigang, K. Maki, C. Otani, and K. Kawase, Appl. Phys. Lett. **88**, 071122 (2006).
[20] A. Nahata, A. S. Weling, and T. F. Heinz, Appl. Phys. Lett. **69**, 2321 (1996).
[21] T. Loffler, T. Hahn, M. Thomson, F. Jacob, and H. G. Roskos, Opt. Express **13**, 5353 (2005).
[22] J. Faure, J. van Tilborg, R. A. Kaindl, and W. P. Leemans, Opt. Quantum Electron. **36**, 681 (2004).
[23] Y. J. Ding, Opt. Lett. **29**, 2650 (2004).
[24] K. Wynne and J. J. Carey, Opt. Commun. **256**, 400 (2005).
[25] J. R. Morris and Y. R. Shen, Phys. Rev. A **15**, 1143 (1977).
[26] J. Z. Xu and X.-C. Zhang, Opt. Lett. **27**, 1067 (2002).
[27] V. Ya. Gaivoronskii, M. M. Nazarov, D. A. Sapozhnikov, E. V. Shepelyavyi, S. A. Shkel'nyuk, A. P. Shkurinov, and A. V. Shuvaev, Quantum Electron. **35**, 407 (2005) [Kvantovaya Elektron. (Moscow) **35**, 407 (2005)].
[28] G. L. Dakovski, B. Kubera, and J. Shan, J. Opt. Soc. Am. B **22**, 1667 (2005).
[29] A. Schneider, M. Neis, M. Stillhart, B. Ruiz, R. U. A. Khan, and P. Gunter, J. Opt. Soc. Am. B **23**, 1822 (2006).
[30] D. Cote, J. E. Sipe, and H. M. van Driel, J. Opt. Soc. Am. B **20**, 1374 (2003).
[31] D. A. Kleinman and D. H. Auston, IEEE J. Quantum Electron. **20**, 964 (1984).
[32] A. G. Stepanov, J. Hebling, and J. Kuhl, Appl. Phys. B: Lasers Opt. **81**, 23 (2005).
[33] R. M. Koehl, S. Adachi, and K. A. Nelson, J. Phys. Chem. A **103**, 10260 (1999).
[34] D. H. Auston, Appl. Phys. Lett. **43**, 713 (1983).
[35] M. I. Bakunov, A. V. Maslov, and S. B. Bodrov, J. Appl. Phys. **98**, 033101 (2005).
[36] M. I. Bakunov, A. V. Maslov, and S. B. Bodrov, Opt. Photonics News **16**, 29 (2005).
[37] M. I. Bakunov, A. V. Maslov, and S. B. Bodrov, J. Appl. Phys. **100**, 026106 (2006).
[38] M. I. Bakunov, A. V. Maslov, and S. B. Bodrov, Phys. Rev. B **72**, 195336 (2005).
[39] G. Gallot, J. Zhang, R. W. McGowan, T.-I. Jeon, and D. Grischkowsky, Appl. Phys. Lett. **74**, 3450 (1999).
[40] M. Schall, M. Walther, and P. U. Jepsen, Phys. Rev. B **64**, 094301 (2001).
[41] D. W. Ward, E. Statz, N. Stoyanov, and K. A. Nelson, in *Engineered Porosity for Microphotonics and Plasmonics*, MRS Symposium Proceedings No. 762, edited by R. Wehrspohn, F. Garcial-Vidal, M. Notomi, and A. Scherer (Materials Research Society, Pittsburgh, PA, 2003), pp. C11.60.1–C11.60.6.

[42] N. S. Stoyanov, T. Feurer, D. W. Ward, E. R. Statz, and K. A. Nelson, Opt. Express **12**, 2387 (2004).

[43] To convert the nonlinear coefficients d_{33} and d_{14} given in SI to cgs, one should use the following rule: $d[\mathrm{cm/cgse}]=(3\times10^{-8}/4\pi)d[\mathrm{pm/V}]$.

[44] W. J. Moore and R. T. Holm, J. Appl. Phys. **80**, 6939 (1996).

[45] Q. Chen, M. Tani, Z. Jiang, and X.-C. Zhang, J. Opt. Soc. Am. B **18**, 823 (2001).

[46] M. I. Bakunov, S. B. Bodrov, A. V. Maslov, and A. M. Sergeev, Phys. Rev. E **70**, 016401 (2004).